Characterizing Transient Regime Multi-frequency Raman Generation

by the Aid of Spectral Phase Interferometry for Direct Electric-field Reconstruction

by

Hao Yan

A thesis

presented to the University of Waterloo

in fulfilment of the

thesis requirement for the degree of

Master of Science

in

Physics

Waterloo, Ontario, Canada, 2013

I hereby declare that I am the sole author of this thesis. This is a true copy of the thesis, including any required final revisions, as accepted by my examiners.

I understand that my thesis may be made electronically available to the public.

Abstract

Multi-frequency Raman Generation (MRG) has been achieved in the transient regime excited by dual-wavelength chirped pump pulses. Spectral phase interferometry for direct electric-field reconstruction (SPIDER) technique is used to study the group velocity dispersion (GVD) of MRG. A few changes have been applied to the SPIDER set-up to adapt it to the multi-color but narrow-bandwidth pulses. The phase of orders from the 1^{st} Stokes order through to the 1^{st} anti-Stokes order are measured. The technique is applied on the study of phase dependency of the 1^{st} anti-Stokes orders on frequency tuning through the Raman transition.

Acknowledgements

First of all, I would like to thank my supervisor Dr. Donna Strickland for offering me the great opportunity to work in her research lab and the help and guidance on my research project.

I also wish to thank Dr. Joe Sanderson for being generous to me lending me all the equipment I needed.

Table of Content

List of Figures

1 Introduction to Multi-frequency Raman Generation (MRG)

Since the development of the laser in 1960, it has been playing an important role in everyday application as well as pushing the frontier of scientific research. It makes it possible for people to control the light as they expect. The energy of laser light can be so concentrated that it changes the optical properties of the medium (Boyd, 2008). Furthermore, a pulsed laser, which is based on the temporal coherence of lasers, allows the instantaneous power of light to reach extremely high levels, and provides high temporal resolution for ultra-fast processes. The frequency tunablity of lasers is determined by the gain mechanism. However, laser sources usually produces narrow bandwidth light only. A lot of effort has been put into generating broad spectra satisfying specific applications.

1.1 General Description of MRG

For our research interest, a broader spectrum means more potential for building ultra-short pulses. Such a spectrum is achieved in our lab through Multi-frequency Raman Generation (MRG), in which several scattered components with different optical frequencies are produced with two-color-pump excitation. Shown in Figure 1-1 (a), in general cases, even with a laser pump, the light is scattered into a few extremely weak frequency components corresponding to each molecular vibrational or rotational state. The frequency difference between the scattered components and the laser pump matches the Raman frequency ω_r. However, with two strong pump beams whose frequency separation is set on resonance with the Raman active medium as shown in Figure 1-1 (b), the process is dramatically enhanced and each scattered component is again scattered into a new frequency. The process will keep going, generating more than 10 Raman orders. The Raman orders can spread from the in the whole visible spectrum (Imasaka, T., Kawasaki, S. and Ishibashi, N. , 1989).

Such a spectrum is capable of building ultra-short pulses due to its broad spectrum as well as its phase-locking properties of the produced components (Shigetaka Yoshikawa, Totaro Imasaka, 1993). By saying phase-locking, it means that there is a fixed phase relationship between each Raman order. On the contrary, the white light from an incoherent light source has a very broad spectrum, but it cannot be used to build ultra-short pulses because of the random phase of each frequency. Since the frequency of the MRG spectrum is discrete, the phase of each component can be put together by adding a certain delay to each order. Then a chain of ultra-short pulses is generated as shown in

Figure 1-2. Compared to ultra-short pulse generation from MRG, the competing technique of continuum generation brings the problem on how to deal with the dispersion over a broad spectrum.

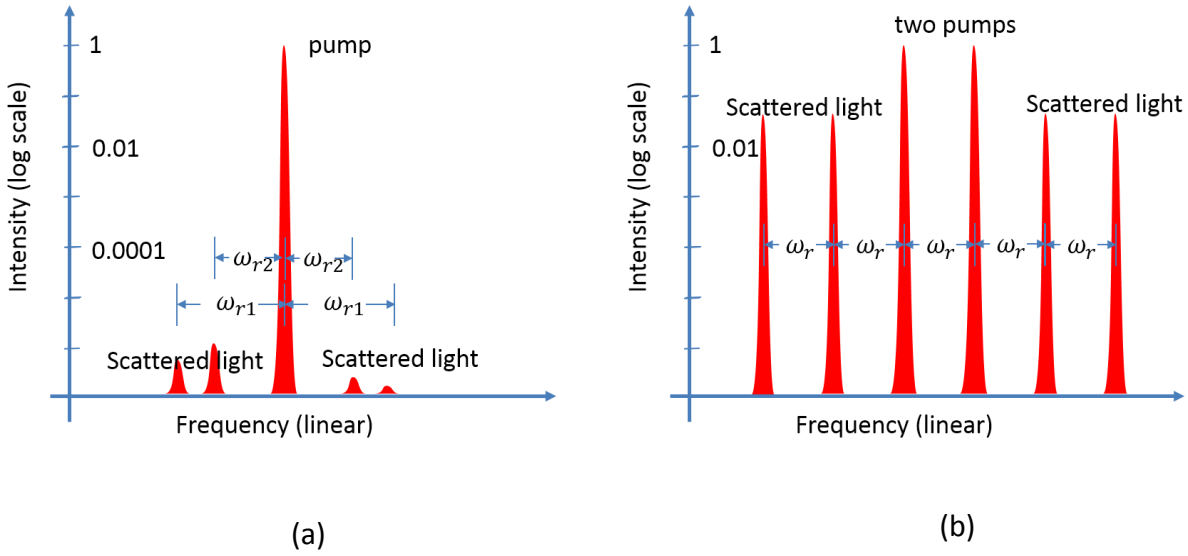

Figure 1-1 Spectrum of Raman scattering. (a) Spontaneous Raman scattering (b) Stimulated multi-frequency Raman Generation

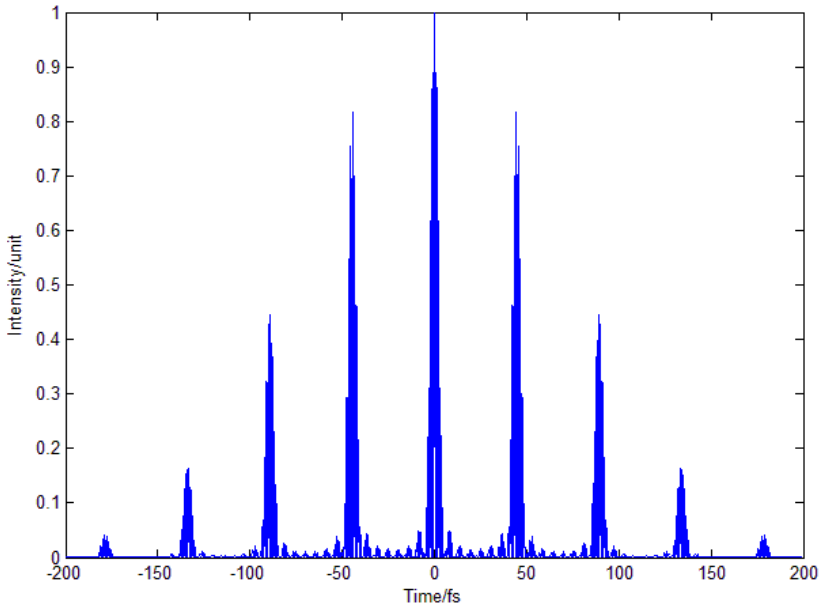

Figure 1-2 A chain of ultra-short pulses built from transient regime MRG

In the early days, experiments on MRG for ultra-short pulse generation were done in the adiabatic regime where the duration of the pump pulses and sidebands are much longer than the dephasing time T_2 of the Raman medium. It was demonstrated that generating a long chain of 2 fs optical pulses had been achieved by mixing 5 Raman orders together (Sokolov, A. V. and Harris, E. et al, 2001).

The energy of the chain of ultra-short pulses is spread out in the adiabatic regime MRG. To achieve more peak intensity, MRG for ultra-short pulses generation experiments are moved forward to the transient regime (Losev, L. L. et al, 2002) and the impulsive regime (Zhavoronkov, N. and Korn, G., 2002). When the durations of the pump pulses are shorter than the dephasing time T_2 of the molecules, which is typically from multiple picoseconds to multiple nanoseconds, all frequency components become highly coherent. That makes coherent control possible in these two regimes. In the transient regime, the durations of the two pumps are longer than the vibrational cycle of the molecule. Distinguished from the transient regime, impulsive excitation involves a single pulse that is shorter than the vibrational cycle (Yan Y. et al, 1985). Such a pulse has a spectrum so broad that the frequency separation that matches the resonance of the molecule is within its spectrum.

In our lab, the MRG is in the transient regime and the Raman medium (SF_6 gas) and the optical pumps are contained inside a hollow fiber shown in Figure 1-3. Our laser produces optical pulses with 5nm bandwidth centred at 780 and 830 nm. This bandwidth allows the duration of the pump pulses to be less than 300 fs. However, the pulses are so short that they suffer from other unwanted nonlinear processes such as self-phase modulation (SPM). The pump pulses for MRG are chirped to 1 ps to reduce those harmful effects. That means by introducing varying group delay to different frequency, the energy of particular frequency travels ahead of others. The instantaneous frequency

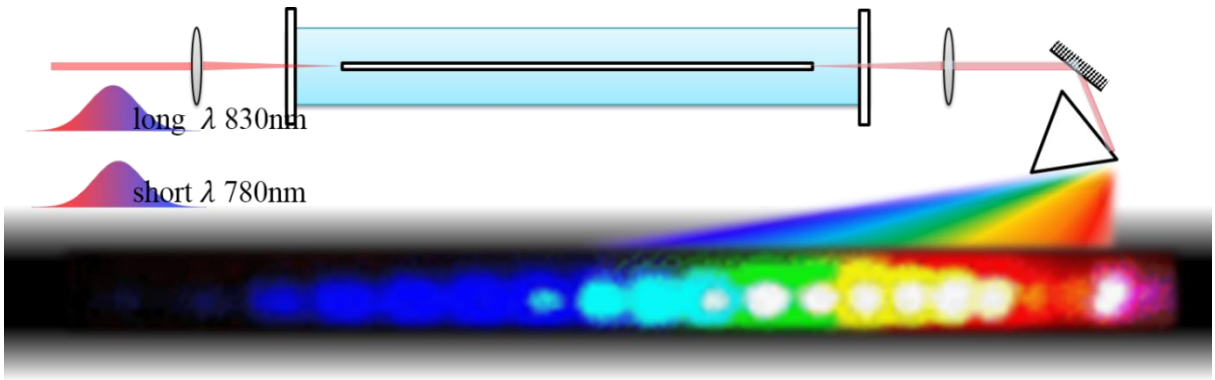

Figure 1-3 Raman cell and MRG

of the pulse is changing from its head to tail and the envelope of the pulse is much longer than the original pulse.

The advantages of using hollowed fiber and chirped pulses have been confirmed by other research groups. It was shown that by containing the gas in a hollow fiber, the efficiency of generating MRG had been greatly improved (Takahashi, E. et al, 2007), and that compared with 50-fs bandwidth limited pulses pumping, the conversion efficiency and number of sidebands had been both increased with chirped pulses pumping (Zhi, M. and Sokolov, A. , 2012). A simulation had been done for our MRG in Turner's thesis (Turner, 2006). It showed that our MRG spectrum is capable of building 3.2fs, $120\mu J$ ultra-short pulses.

1.2 Research Interest

Since the Raman active medium is pumped in the transient regime with chirped pulses, the Raman orders are expected to be chirped pulses as well because the Raman orders are phase-locked with the pumps. We have to compress those chirped Raman orders before mixing them together to build the ultra-short pulses. Only when these chirped order are well compressed, is the energy concentrated. However, pulse compression is not an easy task unless we have enough knowledge of the chirp, which is related to the phase information of the pulse's spectrum. We reintroduce the spectral phase interferometry for direct electric-field reconstruction (SPIDER), which was originally designed to tell the phase information of a 100 fs optical pulse that has central wavelength of 800nm, to study the phase information of the Raman orders under different situations. Several modifications have been made to enable SPIDER measurements on different narrow bandwidth pulses in a wide frequency range.

Exciting the MRG process by chirped pump pulses reduces the unwanted nonlinear process as well as provides convenience for studying the impact of frequency detuning. Shown in Figure 1-4 (a), the two pump pulses are both positively chirped. The low frequency travels ahead of the others. By adjusting the delay on the high frequency beam (780nm), the instantaneous frequency difference between the two pulses changes. When the central frequency separation of the two pulses matches the Raman transition, by making the 780nm pulse be ahead in time, the frequency gap is higher than the Raman transition frequency. Such a configuration is called 'blue-detuning'. On the contrary, the MRG is red-detuned when the 780 pulse is left behind. For negatively chirped pulse in (b), the situation is similar but with the opposite timing.

Previous experiments show that with red-detuning on positively chirped pump pulses, the Raman orders at and below 735nm experience red-shifting (Cui, Z. and Strickland, D. et al, 2013). The spectrum of each order also shows broadening. As far as we know, there is no published mathematical model that completely explains this phenomenon. We hope the study on phase information can bring our understanding to a higher level.

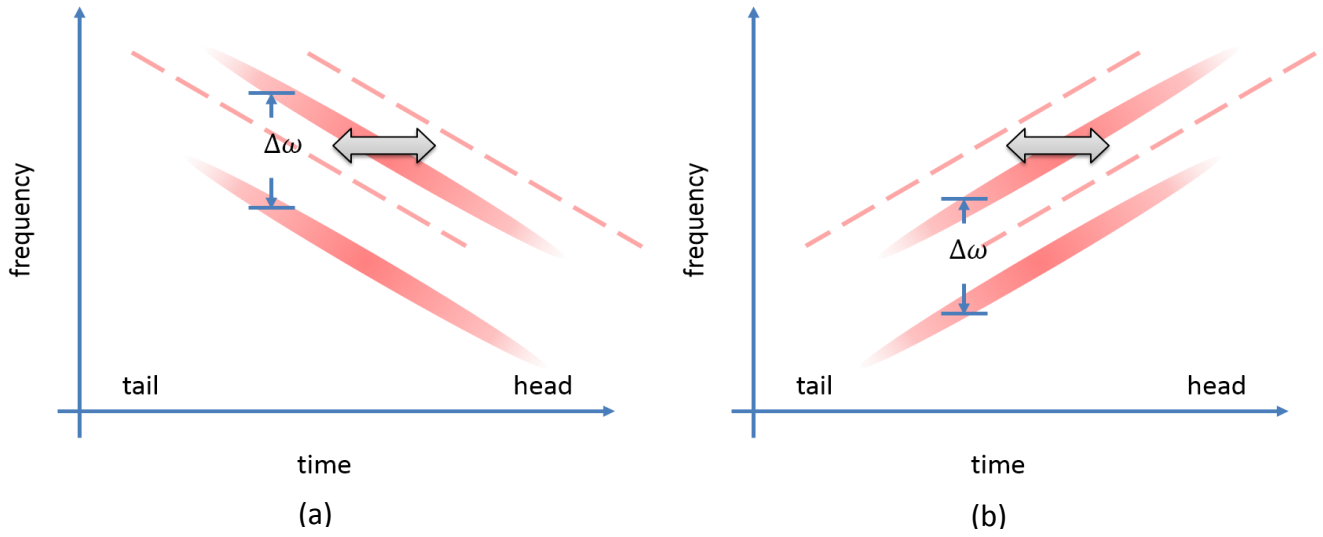

Figure 1-4 Diagram for frequency detune with (a) positively chirped pulses (b) negatively chirped pulses

It is found that our laser has significant random noise and drift. That means the phase information of the pulses is changing slight different from shot to shot. The averaged phase curve is also varying. Besides the study in MRG, we tried to reduce the noise and drift in our laser to get better results in the future.

2 Theory

2.1 Raman Scattering and MRG

Since the discovery by C. V. Raman in 1928 (The Raman Effect, 1998), Raman effect, described as the inelastic scattering of a photon, has been essential in many applications. In Raman scattering, a small portion of the incident light is scattered into different frequencies. The difference in frequency is determined by the interacting material. In other words, there is a certain color change pattern in the scattered light in specific material.

Stimulated Raman scattering is a great source of coherent lights in different frequency. On the other hand, since the spectrum of the scattered light is determined by the material, Raman spectroscopy had been developed to study the chemical compound of material.

2.1.1 General Discretion of Raman Scattering and MRG

Raman scattering involves low energy levels such as vibrational and rotational levels of molecules. The energy of those levels are much lower than the energy of the incident light. Raman scattering can be divided into Stokes scattering and anti-Stokes scattering according to whether the photon loses or gains energy, respectively. A quantum mechanical diagram is shown in Figure 2-1.In Raman Stokes scattering, a molecule is excited by a photon from the ground state to a virtual level associated with real electron state n' and then comes back to a vibrational state n releasing a Stokes photon with lower energy. On the other hand, the scenario for anti-Stokes Raman scattering is that a molecule at vibrational state n absorbs a photon and then decays to the ground state, releasing a photon with higher energy.

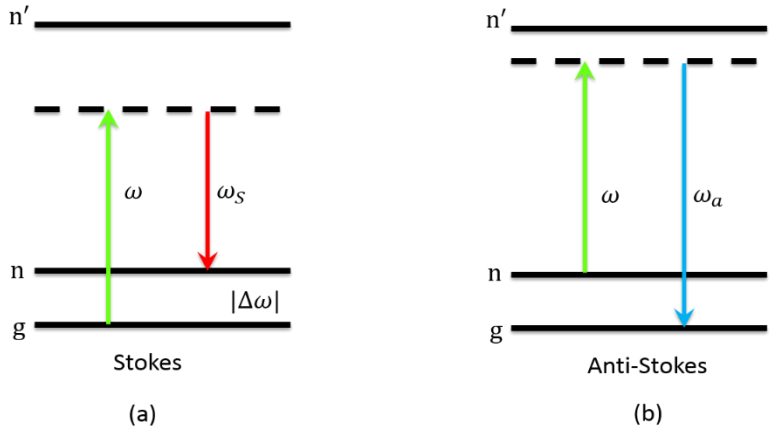

Figure 2-1 Energy level diagram for (a) Stokes Raman scattering (b) anti-Stokes Raman scattering

With a second beam at a Raman resonance from the first beam the vibrational state of the molecule is highly driven and it is coupled with the ground state. The Raman scattering is enhanced when this specific condition is achieved. A large portion of high frequency photon at ω_{L2} is scattered into anti-Stokes frequency ω_{a1}, and the photons at ω_{a1} are again scattered to ω_{a2}. This process keeps going until the limit is reached. A number of Stokes orders can be generated in a similar way.

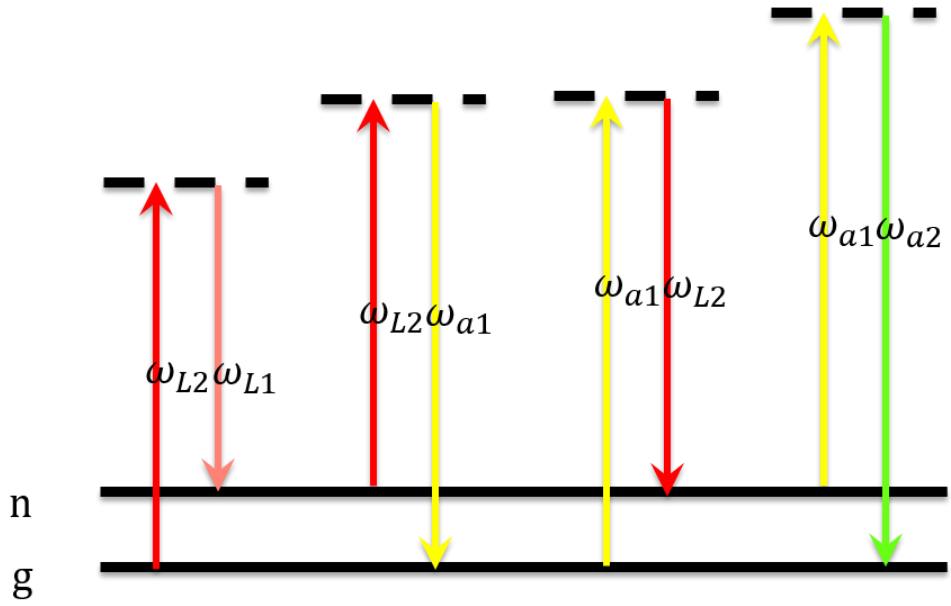

Figure 2-2 Energy level diagram for MRG

2.1.2 Mechanism of Stimulated Raman Scattering

Generally speaking, spontaneous Raman scattering is very weak compared to the original beam. The scattering cross section per unit volume for Raman Stokes scattering is only about $10^{-6}cm^{-1}$ (Boyd, 2008). However, if a second beam at Stokes or anti-Stokes frequency stimulates the process, the Raman scattering process can be strong under certain condition.

The classic approach for studying stimulated Raman scattering involves introducing a simple harmonic oscillator model and solving nonlinear wave equations (Boyd, 2008). The equation of motion for the molecule is

$$\frac{d^2\tilde{q}}{dt^2} + 2\gamma\frac{d\tilde{q}}{dt} + \omega_v^2\tilde{q} = \frac{\tilde{F}(t)}{m}$$

Where $\tilde{q}(t)$ is the deviation of the internuclear distance from its equilibrium, ω_v is the resonance frequency, γ is the damping constant and $\tilde{F}(t)$ is the driving force.

To find the driving force $\tilde{F}(t)$, we need to look into the dipole moment of a molecule located at coordinate z

$$\tilde{\mathbf{p}}(z,t) = \epsilon_0\alpha\tilde{\mathbf{E}}(z,t)$$

Where α is the optical polarizability of the molecule depending on the internuclear separation $\tilde{q}(t)$

$$\tilde{\alpha}(t) = \alpha_0 + \left(\frac{\partial\alpha}{\partial q}\right)_0 \tilde{q}(t)$$

To establish the oscillating dipole moment, a certain amount of energy is needed. That is given by

$$W = \frac{1}{2}\langle\tilde{\mathbf{p}}(z,t)\cdot\tilde{\mathbf{E}}(z,t)\rangle = \frac{1}{2}\epsilon_0\alpha\langle\tilde{\mathbf{E}}^2(z,t)\rangle$$

where the angular brackets denote a time average over an optical period, during which, the slowly varying polarizability α can be considered as a constant. The driving force is given by

$$\tilde{F} = \frac{dW}{dq} = \frac{\epsilon_0}{2}\left(\frac{d\alpha}{dq}\right)_0 \langle\tilde{\mathbf{E}}^2(z,t)\rangle$$

With the presence of two optical fields at frequency ω_L and Stokes frequency ω_S, the $\langle\tilde{\mathbf{E}}^2(z,t)\rangle$ term oscillates at the beat frequency $\omega_b = \omega_L - \omega_S$, which is coincident with the Raman frequency ω_v. Thus, the driving force is on resonance of the harmonic oscillator, and the motion of the oscillator is highly excited, leading to a modulation at ω_v through the varying polarizability $\alpha(t)$. The polarization at $\omega_a = \omega_L + \omega_v$ in the material is produced. These polarizations at ω_S and ω_a propagate though the material.

2.1.3 Coupled Equations for Raman Scattering and MRG

To have a quantitative view of the stimulated Raman scattering, we have to establish a model on how the polarization is transmitted through the Raman active medium. Since stimulated Raman scattering is a nonlinear process, the nonlinear wave equation is introduced to solve the problem.

$$-\nabla^2\tilde{\mathbf{E}} + \frac{\epsilon^{(1)}}{c^2}\frac{\partial^2\tilde{\mathbf{E}}}{\partial t^2} = -\frac{1}{\epsilon_0 c^2}\frac{\partial^2\tilde{\mathbf{P}}^{NL}}{\partial t^2}$$

where $\mathrm{n}^2 = \epsilon^{(1)}$ and $\widetilde{\mathbf{P}}^{NL}$ is the nonlinear polarization. The electric field is

$$\tilde{\mathbf{E}}(z,t) = \sum_i A_i e^{i(k_i z - \omega_i t)} + \mathrm{c.c}$$

where c.c is the complex conjugate term. By substituting the electric field in to the expression for driving force and solving the equation of motion of the harmonic oscillator, the amplitude of the vibration is given by

$$\mathrm{q}(\Omega) = \frac{(\epsilon_0/m)(\partial\alpha/\partial q)_0}{\omega_v^2 - \Omega^2 - 2i\Omega\gamma} \sum_{\omega_\mathrm{i}-\omega_\mathrm{j}=\omega_v} A_i A_j^*$$

where $\Omega = \omega_L - \omega_S$. thus,

$$\widetilde{\mathbf{P}}^{NL} = \epsilon_0 N \left(\frac{\partial\alpha}{\partial q}\right)_0 \sum_{\omega_\mathrm{i}-\omega_\mathrm{j}=\omega_v} \left[\mathrm{q}(\Omega) e^{i(k_i-k_j)z - i\Omega t} + c.c\right] (A_i e^{i(k_i z - \omega_i t)} + A_j e^{i(k_j z - \omega_i t)} + c.c)$$

The polarization of each Raman order is coupled with its two neighbor orders. As a consequence, the polarization oscillating at all Raman frequencies are coupled together. The phase relationship is then fixed.

By substituting $\mathbf{P}$ and $\mathbf{E}$ into the nonlinear wave equation and equating terms with the same frequency, we have

$$-\frac{\partial^2 E_i}{\partial \mathrm{z}^2} \mathrm{e}^{-i(k_i z - \omega_i t)} + 2ik_i \frac{\partial E_i}{\partial z} e^{-i(k_i z - \omega_i t)} + \mathrm{k_i^2} E_i e^{-i(k_i z - \omega_i t)} - \frac{\epsilon^{(1)}\omega_i^2}{c^2} E_i e^{-i(k_i z - \omega_i t)} + c.c$$
$$= \frac{N\omega_i^2}{c^2} \left(\frac{\partial\alpha}{\partial q}\right)_0 (q(z) E_{i-1} + q^*(z) E_{i+1}) e^{-i(k_i z - \omega_i t)} + c.c$$

The third and fourth term cancel each other. When the envelope is varying so slowly that we can consider it as a constant in a single wavelength scale (our case), the slowly-varying envelope approximation is applied. Thus the first term vanishes.

The final expression gives

$$\frac{\partial E_i}{\partial z} = -\frac{iN\omega_i}{2n(\omega_i)c} \left(\frac{\partial\alpha}{\partial q}\right)_0 \left(\tilde{q}(z,t)\mathrm{E_{i-1}} e^{i(\boldsymbol{k_n} - \boldsymbol{k_{n-1}})z} + \tilde{q}^*(z,t)\mathrm{E_{i+1}} e^{i(\boldsymbol{k_{n+1}} - \boldsymbol{k_n})z}\right)$$

where

$$\mathrm{q(z,t)} = \frac{1}{4}\frac{(\epsilon_0/m)(\partial\alpha/\partial q)_0}{\omega_v^2 - \Omega^2 - 2i\Omega\gamma} \sum_{\omega_\mathrm{i}-\omega_\mathrm{j}=\omega_v} E_i E_j^* \, e^{-i(\boldsymbol{k_n}-\boldsymbol{k_{n-1}})z}$$

2.1.4 Phase-Matching Condition

The previous sections show that the polarization oscillating at the Raman frequency exists and propagates in the material, but it does not guarantee the growth of the amplitude of the Raman orders. In fact, the intensity of beams generated by nonlinear processes such as second harmonic generation (SHG) and sum frequency generation (SFG) is always low if the phase-matching condition is not reached. The phase-matching condition is also important in anti-Stokes MRG.

The phase-matching condition is like a momentum conservation law in phonics. The momentum of a photon is proportional to its wavevector $\boldsymbol{k}$

$$\boldsymbol{p} = \hbar\boldsymbol{k} = \frac{\mathbf{h}}{\lambda}\hat{\mathrm{n}}$$

where $\hat{\mathrm{n}}$ points at the direction of $\boldsymbol{k}$. For stimulated Raman and sum frequency generation to massively happen, the difference in sum $\boldsymbol{k}$ between initial and final states (so called phase mismatch $\Delta\boldsymbol{k}$) must vanish. In vacuum, when all components are collinear, it is obvious that

$$\Delta\boldsymbol{k} = \boldsymbol{k}_{aS} + \boldsymbol{k}_S - 2\boldsymbol{k}_{pump} = \left(\frac{2\pi}{\lambda_{aS}} + \frac{2\pi}{\lambda_S} - 2\frac{2\pi}{\lambda_{pump}}\right)\hat{\mathrm{n}} = \mathbf{0}$$

However, in a medium with nonlinearity, there is dispersion. Thus the wavevector becomes

$$\boldsymbol{k} = \frac{2\pi}{n(\lambda)\lambda}\hat{\mathrm{n}}$$

where $n(\lambda)$ is the wavelength-dependent refractive index, $\Delta\boldsymbol{k}$ does not vanish in most cases. Phase-matching can be achieved in medium through angle tuning. In crystals with birefringence the refractive index is also dependent on the angle of incidence for beam with extraordinary polarization. The phase-matching condition can be achieved with specified angular configuration. Fortunately, the anti-Stokes MRG could still occur with small phase mismatch (Aussenegg, 1983). It happens collinearly in gas, where the dispersion is low.

2.2 Group Velocity Dispersion

Group velocity dispersion (GVD) is essential in the study of ultra-fast optics. The duration of a short pulse is highly dependent on the GVD in its path. For instance, when a broadband, transform-limited pulse is propagating through a piece of glass, the energy of each frequency component travels at $v_g = \frac{\partial \omega}{\partial k}$. Due to the normal GVD, the energy of low frequency component is traveling faster than the energy of high frequency component. As a consequence, the pulse is getting longer through media such as glass and water. The instantaneous frequency is low at the front of the pulse and high at the end of the pulse.

Similarly, there is GVD through grating pairs, where angular dispersion occurs, caused by the difference in optical path for the various frequency components. In the set-up in Figure 2-3(a), the group delay of the short wavelength component is less than those of longer wavelength. In the end, the energy of short wavelength color passes through the compressor faster than others. Such a set-up is of positive group velocity dispersion. The one in (b) has either positive or negative dispersion with different configuration.

The GVD for a grating pair is

$$\frac{\partial \tau}{\partial \lambda} = \frac{\lambda b}{c d^2 \cos^2 \theta_D}$$

where $b = l_1 + l_2 - 2f$ for the set-up with focusing lens, d is grating constant, and θ_D is the angle of incident on grating (Weiner, 2009).

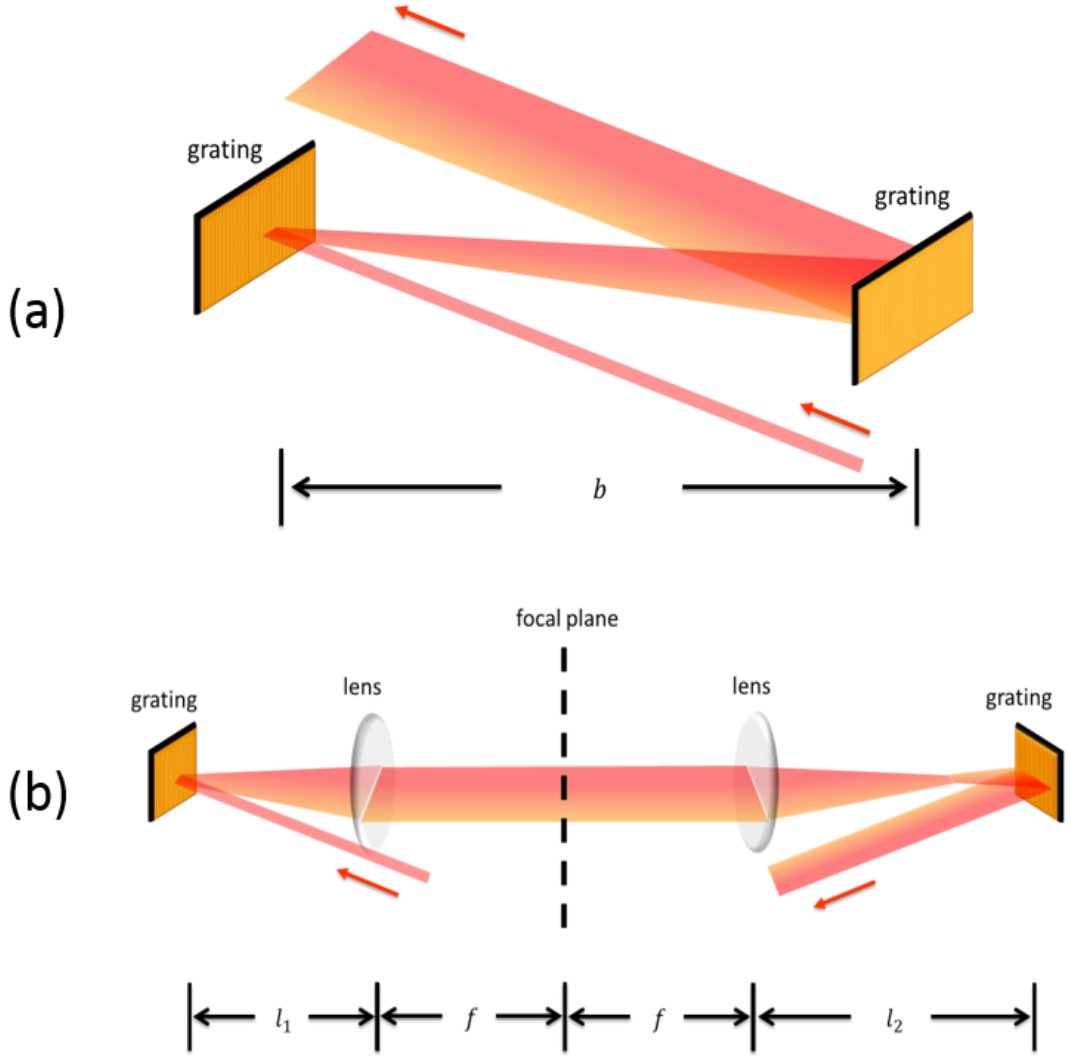

Figure 2-3 (a) Grating pair with negative GVD (b) Grating pair with internal lenses

An anti-parallel prism pair is shown in Figure 2-4. The dispersion in prism pairs is more complicated since it has both angular and material dispersion. With large spacing, the normal GVD caused by material dispersion is overwhelmed by the angular dispersion. Thus, the anomalous dispersion takes over. The advantage of using prisms is the lower energy loss on prisms than on gratings. However, for the same amount of linear chirp, there is more higher order dispersion in a prism compressor and it requires more spacing than a grating compressor.

In most cases, a mirror is placed the end of the optical paths in Figure 2-3, and Figure 2-4. The beam will be reflected all the way back to reduce spatial chirp.

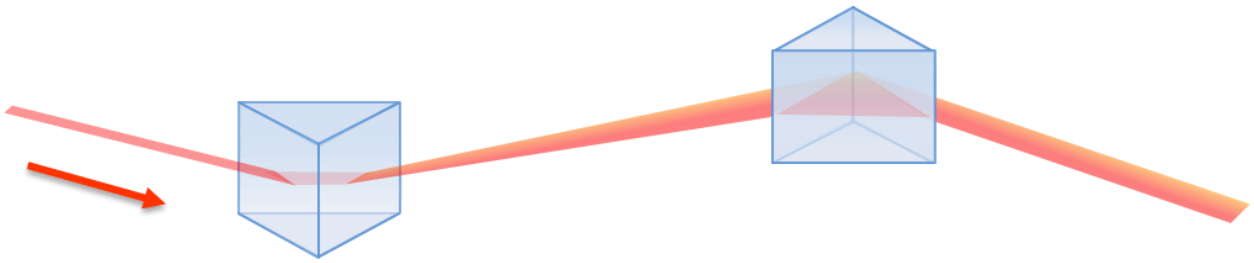

Figure 2-4 Prism Compressor

2.3 Phase Information and Chirp

The linear chirp is related to the second order derivative of the phase respect to frequency (Weiner, 2009).

$$\frac{\partial \tau}{\partial \omega} = -\frac{\partial^2 \phi}{\partial \omega^2}$$

As shown in Figure 2-5, the phase of an unchirped pulse is flat or linear to the frequency while the chirped pulse has a quadratic phase curve.

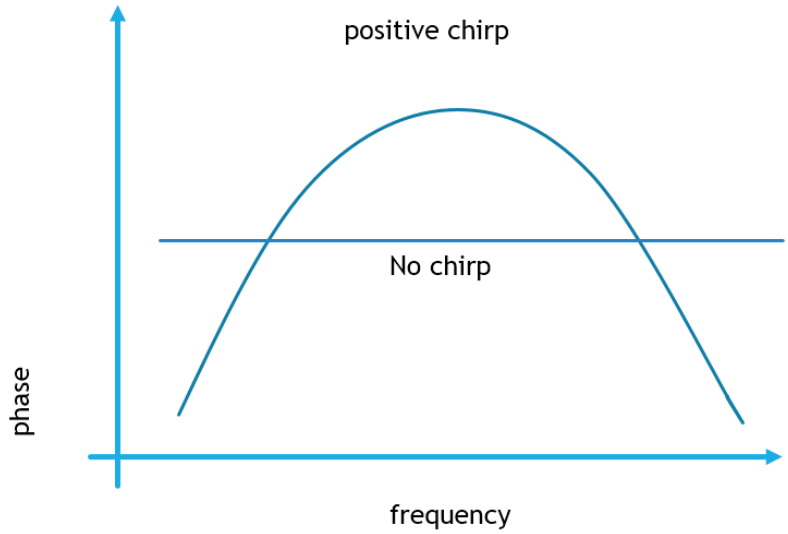

Figure 2-5 The phase curve for positively chirped pulse and unchirped pulse

3 Experimental Apparatus

The whole optical system for studying MRG can be divided into the following parts as shown in Figure 3-1. Two optical pulses with different central wavelength are generated and amplified through the Dual-wavelength Chirped Pulse Amplification System. The two pulses act as a pump to drive the vibrational state of the molecule inside the hollow fiber assembly to then produce the MRG being studied. There are several diagnostics to help monitor the properties of the laser pulses.

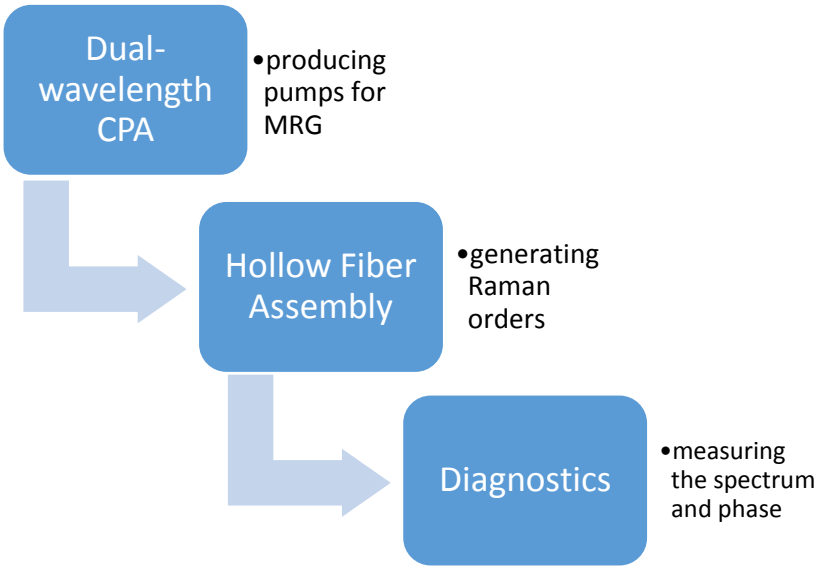

Figure 3-1 A brief diagram of the experimental set-up

3.1 Dual-wavelength Chirped Pulse Amplification System

Chirped-Pulse Amplification, developed by Strickland and Mourou (1985), is a technique to amplify short optical pulses (Strickland, D. and Mourou, G., 1985). The basic idea is to stretch a laser pulse in the time domain by adding linear chirp before amplifying it. Thus, the peak power inside the gain medium is reduced to avoid damage. Once amplified, the long pulse can be compressed by adding opposite chirp.

The dual-wavelength chirped pulse amplification system consists of a broad-band oscillator, a pulse stretcher, a regenerative amplifier (regen), a multi-pass amplifier, and a pulse compressor.

3.1.1 Broad-band Mode-locked Oscillator

There is a commercial mode-locked oscillator in Dr. J. Sanderson's lab. It produces 10 fs pulses by a passive mode-locking mechanism. Inside, there is a Ti:Sapphire crystal pumped by a commercial Nd:YAG laser. Once a perturbation is applied, it will achieve mode-locking through a Kerr lens process. Once the equilibrium is reached, the output of the oscillator is a chain of ultra-short pulses whose repetition rate is 75 MHz, with a central wavelength of 800 nm. The average power of the beam is 400 mW and 50% is sent to the Dual-wavelength CPA as a seeding beam.

3.1.2 Pulse Stretcher

The optical path for the pulse stretcher is shown in Figure 3-3. Before the beam reaches the stretcher, it first arrives at a Faraday isolator, which protects the oscillator from the returning amplified beam. A large portion of the beam propagates through while the other portion is redirected to a fast diode which provides a trigger signal for the regen. We used to send the beam from Dr. Sanderson's lab to ours through an optical fiber, which was found to be an origin of noise of the CPA laser. The beam is now sent directly to the regen through air.

After the Faraday isolator, the seeding beam is split by a prism pair according to its wavelength. Long and short wavelength beams travel along their own paths. Each of them hits the first grating. Next its -1 order diffracted beam is focused by the concave mirror onto the plane mirror, and then goes back to the concave mirror and grating. Then, the beam hits the right-angle mirror and goes all the way back through the grating line back to the first prism and exits the compressor. The design of this pulse stretcher is the equivalent of Figure 2-3(b). It chirps the pulses to hundreds of picoseconds. The calculated instantaneous wavelength over time is shown in Figure 3-2, and the spectrum of the seeding beam is shown in Figure 3-4. After the prism, the seeding beam travels through a ½ wave plate and the second Faraday isolator before entering the regen.

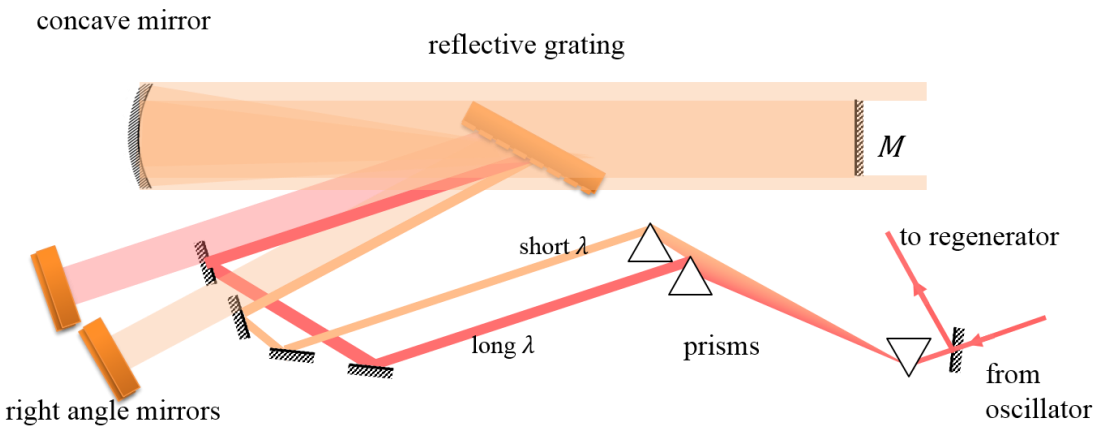

Figure 3-3 Dual-wavelength pulse stretcher

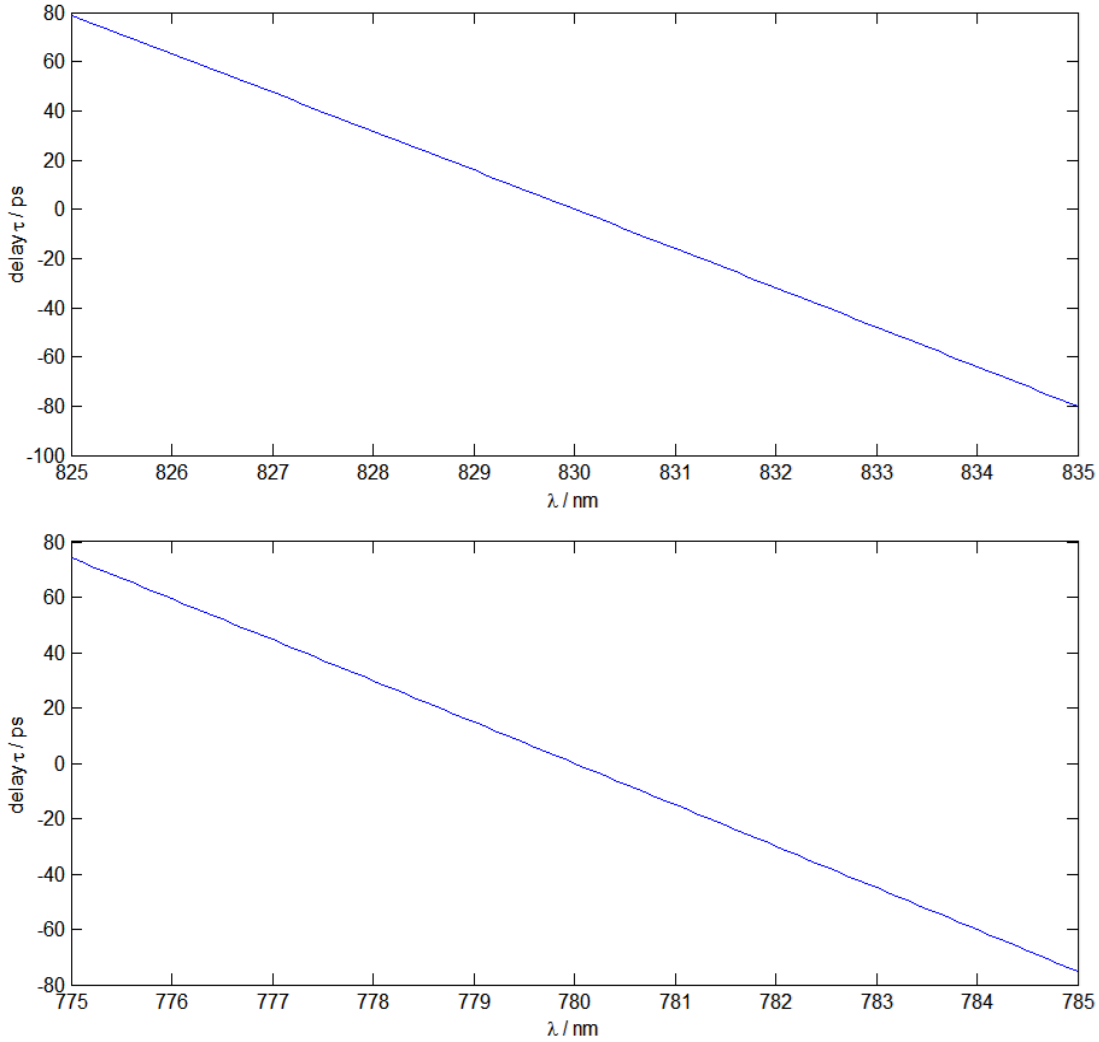

Figure 3-2 Group delay in the pulse stretcher

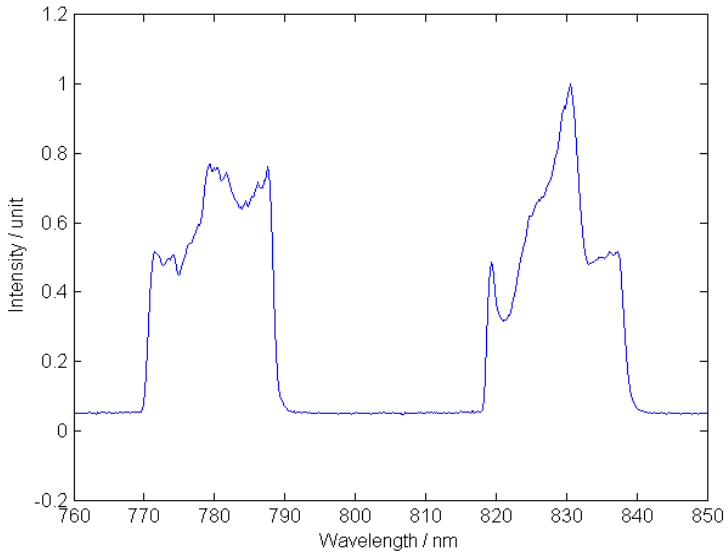

Figure 3-4 The spectrum of the seed beam

3.1.3 Regenerative Amplifier

Shown in Figure 3-5, the dual-wavelength regenerative amplifier (regen) is an X-folded four-mirror cavity. Seeded by a mode-locked oscillator, the regen is capable of amplifying frequency-tunable pulses with energy up to multiple mJ.

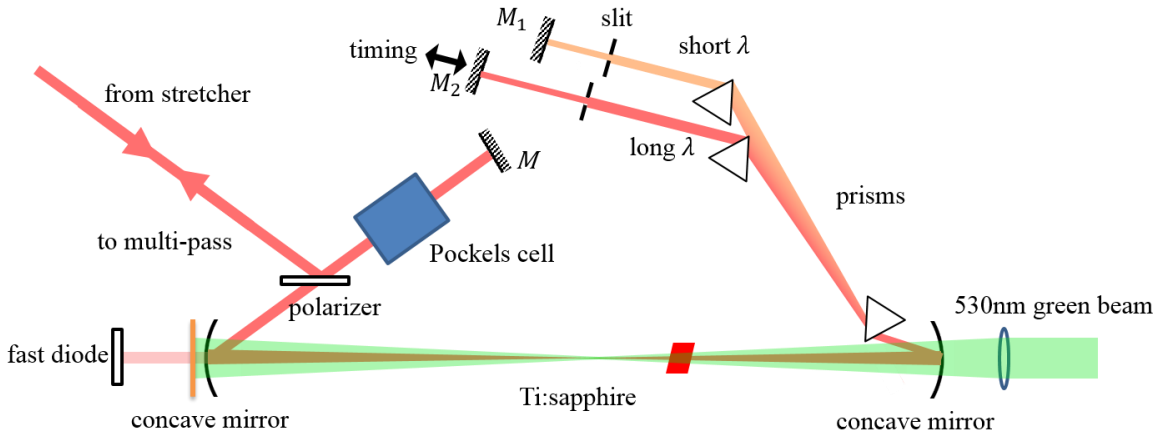

Figure 3-5 Dual-wavelength regenerative amplifier

The gain medium is a Ti:Sapphire laser rod with a Brewster-angle cut and is optically pumped by a frequency-doubled Neodymium-doped Yttrium-Aluminium-Garnet (Nd:YAG) laser pulse from Spectra-Physics. When amplifying, the optical pulses oscillate back and forth between the two plane mirrors. The two concave mirrors stabilize the beam inside the cavity, while the three-prism and slit set-up provides frequency tunability. The back mirror for the long wavelength is mounted on a translational stage for timing to let the two colors have the same round trip time. The optical switch that controls the beam entry and exit of the cavity consists of a Medox Pockels Cell, its controller, and a polarizer. Inside the Pockels cell, there is a crystal of birefringence. The refractive index of the ordinary (o) and extraordinary (e) polarizations are dependent on the static electric field. It can act as a quarter wave plate, a half wave plate and a ¾ wave plate when specified voltage is applied to it, switching the polarization of the beam.

The output of regen can be compressed to femtosecond pulses only when it is well seeded. To achieve this, the seeding beam has to be aligned up with the back mirrors of the regen. At the beginning of an amplifying cycle, the frequency doubled Nd:YAG laser sends an optical pulse to pump the Ti:Sapphire rod. Meanwhile, the Pockels cell is in Q-switch mode which means it is of low cavity gain preventing the regen from lasing. The s-polarized seeding pulse enters the regen after reflected by the polarizer. After it passes through the voltage-off Pockels Cell, which is equivalent to a quarter wave plate, twice, it becomes p-polarized and passes through the polarizer. When the seeding pulse comes back again, it will be switched back to s-polarized again and leave the cavity without absorbing much energy on the laser rod. When the Ti:Sapphire crystal is well pumped, the cavity is ready for amplifying the seed pulses and is waiting for one to come in. Before the second pulse enters the Pockels cell, as well as before the p-polarized pulses comes to the Pockels cell again, the controller, which is triggered by the pump pulse and timed to 2ns by the mode-locked pulse signal, sends a voltage pulse to the Pockels cell, converting it to a half wave plate. Thus, the p-polarized pulse is locked in the regen, absorbing the energy from the pumped rod, while the following s-polarized pulses cannot enter the regen. At a specified time, which is usually when most energy has been transferred from the laser rod to the pulse, the controller sends another voltage pulse to the Pockles cell. Then, the Pockles cell becomes a ¾ wave plate and switches the polarization of the amplified pulse from p to s. Finally, the pulse exits the regen at the polarizer and the Pockels cell is grounded for the next cycle.

To monitor the condition of the regen, a fast diode is placed behind the right concave mirror, on which a small amount of beam passes through. Figure 3-6 (a) shows the waveform when the regen is well seeded. The sharp spikes represents the amplified pulses, while the background represents the amplified spontaneous emission (ASE).

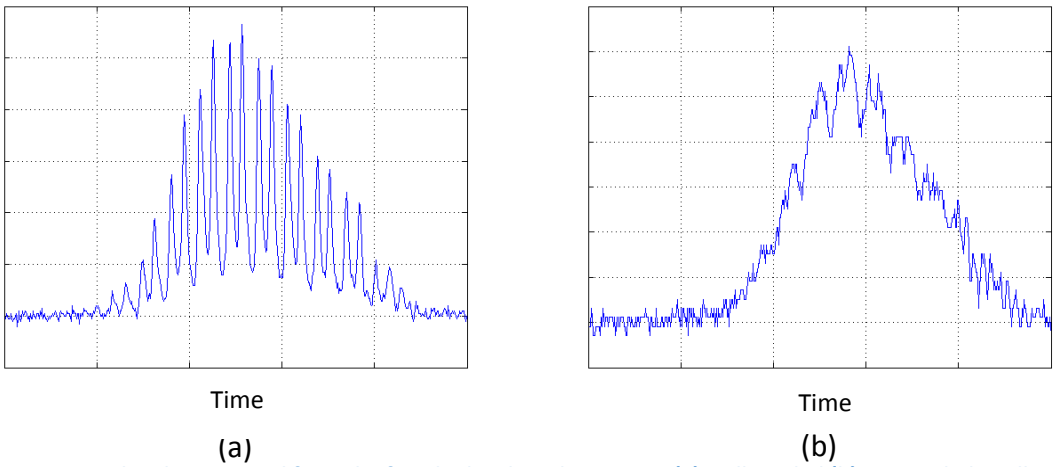

Figure 3-6 The electric signal from the fast diode when the regen is (a) well seeded (b) not seeded at all

3.1.4 Multi-pass Amplifier

After the regen, a second cavity-free amplifier, shown in Figure 3-7, is capable of boosting the energy per pulse for at most 10 times. Guided by mirrors, the pulses that come from regen pass through the Ti:Sapphire rod 5 times. The optical pump comes from the same Nd:YAG laser as for the regen, with 10 percent of the energy pumping the regen and the rest pumping the multi-pass amplifier. The 90 percent beam is split by a 50% beam splitter to pump the laser rod in both directions. The focal

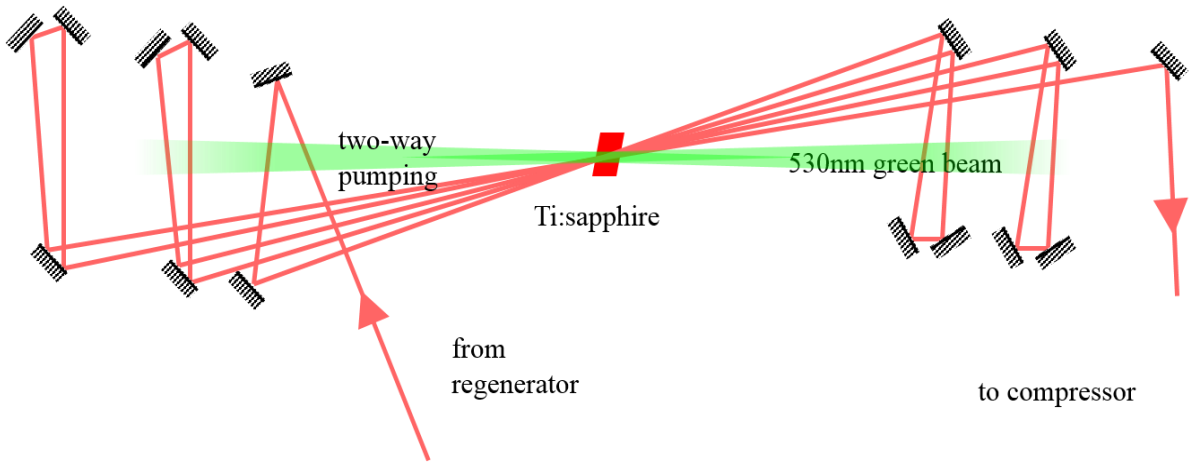

Figure 3-7 The multi-pass amplifier

points for both directions are behind the rod to avoid damaging. When the pump is not turned on, the loss is 50% due to the reflection on the laser rod and diffraction from the growing beam size.

3.1.5 Pulse Compressor

The pulse out of the amplifier has to be re-compressed for follow-up experiments. Figure 3-8 shows the pulse compressor that has the opposite GVD to the pulse stretcher to compensate the chirp of the amplified pulses. Having been diffracted by the first grating, the -1 order beam of the long and short wavelengths splits. Each beam is diffracted again by its own second grating and the diverging is stopped. Reflected by the gold rectangular mirrors, the two beams travel all the way back to the first grating and get re-combined. The compressed pulses exit the compressor at M_b, which is lower than M_a. The second gratings are often moved back and forth for appropriate pulse compression, and M_2 is on translational stage for timing.

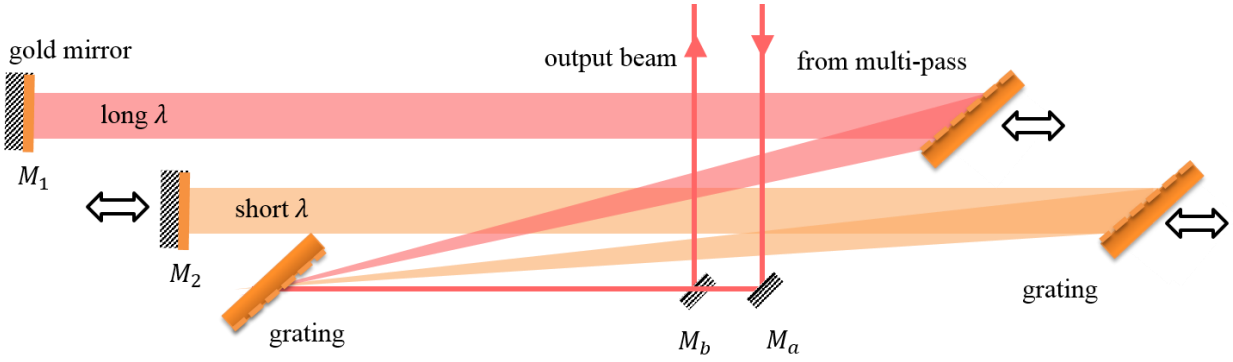

Figure 3-8 Dual-wavelength pulse compressor

After the compressor, the beam is split by a polarizer. The energy distribution can be changed by tweaking the half wave plate in front of the polarizer.

3.1.6 Hollow Fiber Assembly

Extending the length of the beam focus, a hollow fiber assembly provides an ideal place for nonlinear optical processes in gas. In our case, this set-up also makes it easier to collect the MRG light. Nonlinear effects only massively happen with extremely high intensity. In absence of a waveguide, only a small area near the focal point has the intensity exceeding the threshold for MRG.

Like regular optical fiber, the hollow fiber is capable to contain light (Marcatili, E. and Schmeltzer, R., 1964). Though the inner region has lower refractive index than the outer region, the light is trapped inside if the beam is focused into it at a small enough angle. That can be explained by the Fresnel coefficient of a dielectric material: when the angle of incidence is approaching 90%, the reflection on the surface of dielectric material is nearly 100%. This assembly also provides a small dispersive region for the nonlinear processes. The waveguide itself is of negative GVD while the gas inside of positive. In our case, the two compensate each other.

The hollow fiber assembly is shown in Figure 3-9. A 0.5-meter-long hollow fiber with inner diameter of 150 μm is placed into a sealed cylindrical chamber which has two glass windows at the ends for light to go through. A v-groove aluminum bar is inside to seat the fiber. Two lenses for coupling and decoupling are placed right beside the glass windows to minimize the self-phase modulation (SPM) in the glass. To adjust the two ends of the chamber independently, the ends of the cylinder gas chamber are is mounted on two X-Y translational stages. The chamber is connected to a SF_6 gas tank and a vacuum pump.

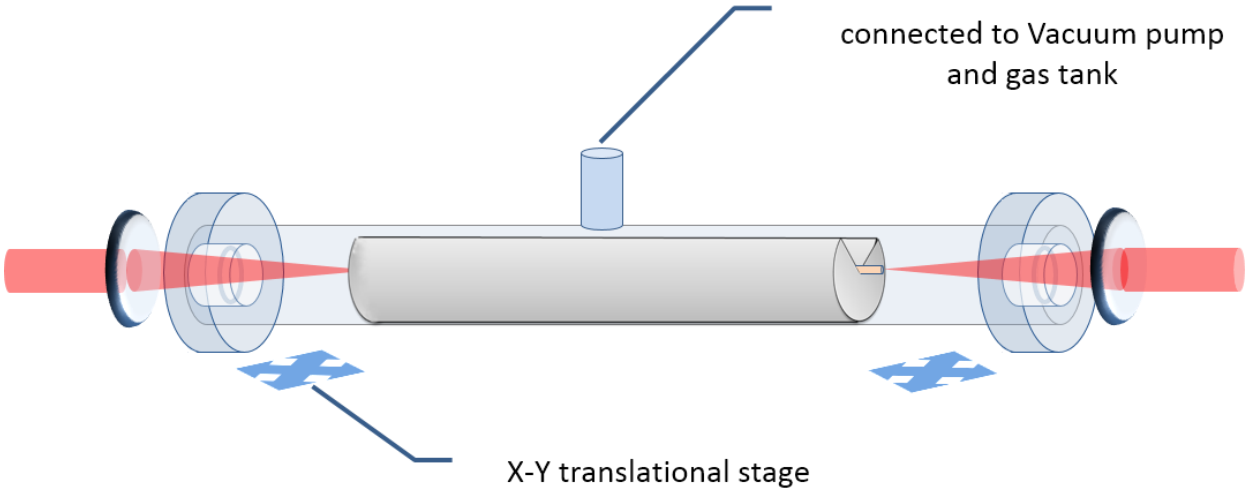

Figure 3-9 Hollow fibre assembly

3.2 Auto-correlator

The method to intuitively measure the time duration of a single color pulse is called autocorrelation. The pulse is split into two beams and these two beams pass through the BBO crystal. Due to the second harmonic generation (SHG) within the crystal, a frequency doubled beam is induced where

the two incoming beams overlap. The auto-correlation trace (Figure 3-10), which is proportional to the duration of the incoming pulse, is captured by a CCD camera. A Labview program reads the image and computes the full-wave half-maximum (FWHM) width in pixels. The program has to be calibrated before use. One need to find the time in femtoseconds per pixel by measuring how many pixels the center of auto-correlation trace moves when a certain delay is added to one beam. Such value is divided by $\sqrt{2}$, to account for the double timing through the delay line. The pulse duration is estimated from the measurement of the FWHM width by dividing by a factor of 1.4, which assumes the pulse shape is Gaussian.

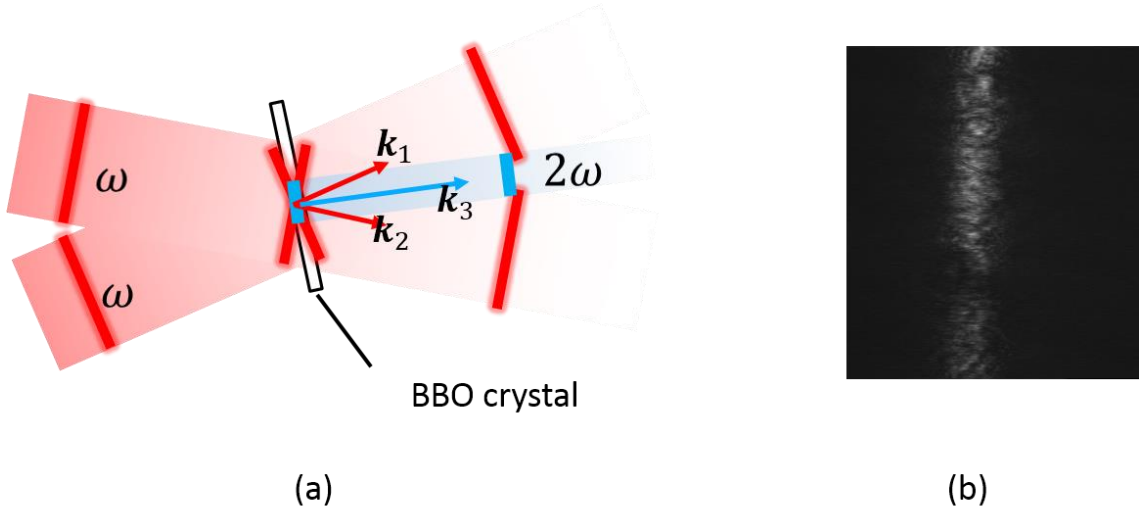

Figure 3-10 (a) SHG on BBO crystal (b) auto-correlation trace

The diagram for SHG on BBO crystal is illustrated in Figure 3-10 (a). Where $\boldsymbol{k}$ denotes the wave vector which is proportional to the momentum of the photon. Since the BBO crystal has birefringence, angle tuning may bring the crystal to a point where the phase mismatch $\boldsymbol{k_3 - k_2 - k_1}$ is zero. Thus the SHG is enhanced and detectable.

The auto-correlator is capable for cross-correlation between long and short wavelength pumps. The angle tuning is the midpoint between the one for auto-correlation on short wavelength pulse and the one on long wavelength pulse. If the two pumps are both aligned with the auto-correlator, and sum-frequency generation (SFG) is phase-matched, the cross-correlation trace will show up when the back mirror in compressor is moved to temporally overlap the two pulses.

3.3 Description of Spectral Phase Interferometry for Direct Electric-field Reconstruction

Measuring the phase of the spectrum of a laser pulse is not an easy task since there is no electronic device which can handle the electric-field oscillation at that high frequency. Fortunately, there are some indirect techniques that can be used to study the phase information.

In 1998, the spectral phase interferometry for direct electric-field reconstruction (SPIDER) was used to measure the second and higher order phase information, which, along with the spectrum, determines the shape and instantaneous frequency of the pulses (Iaconis, C. and Walmsley, I., 1998). SPIDER has complexities in its optical path because SPIDER is an interferometric measurement technique. To retrieve the phase, the interfered spectrum of two pulses with slight different frequency modulation is measured. The physical set-up of SPIDER has a Michelson Interferometer, a pulse stretcher and a nonlinear crystal. The Michelson duplicates the target pulse into two replicas propagating in the same direction with delay τ. The stretched pulse that is much longer than delay τ is the source of the different frequency modulation. The frequency difference is then added to the former two pulse-replicas at the nonlinear crystal through SFG. The two SFG pulses interfere with each other. The interfered spectrum is collected by a high resolution spectrometer for phase retrieving. The frequency-doubled pulse replica is measured for calculating the delay τ.

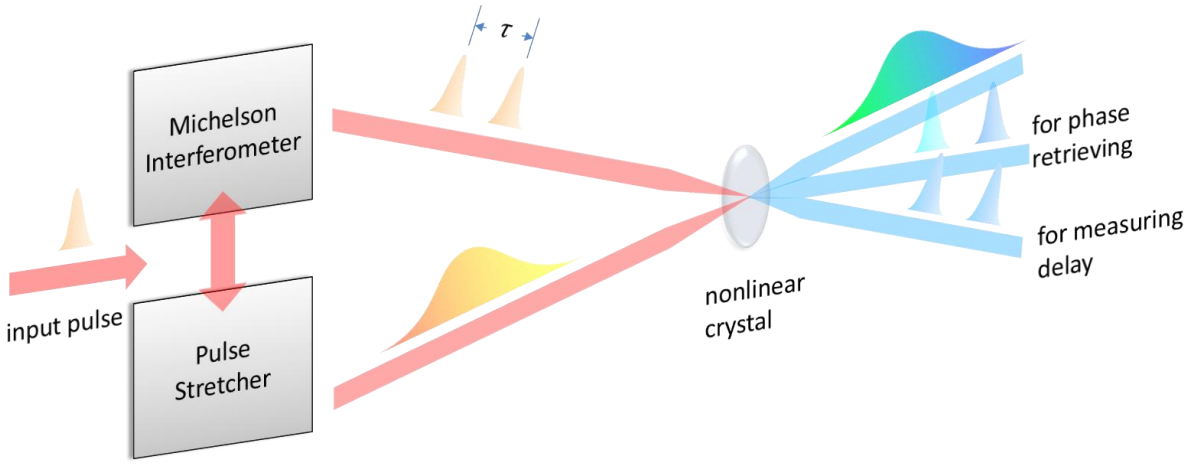

Figure 3-11 A diagram for SPIDER optical path

The signal for a SPIDER measurement is a spectrum with several fringes due to the spectral interference between two SFG pulses. Consider two identical pulses $E(\omega)$ separated by τ in time

domain are up converted to $E'(\omega)$ and $E'(\omega-\Omega)$. The difference in frequency Ω comes from the delay when cross-correlating with the chirped referencing beam. The standard shearing interferogram $D(\omega_c)$ is

$$D(\omega_c) = \left|\tilde{E}(\omega_c-\Omega)\right|^2 + \left|\tilde{E}(\omega_c)\right|^2 + 2\left|\tilde{E}(\omega_c-\Omega)\tilde{E}(\omega_c)\right|\cos[\phi_\omega(\omega_c-\Omega)-\phi_\omega(\omega_c)-\tau\omega_c]$$

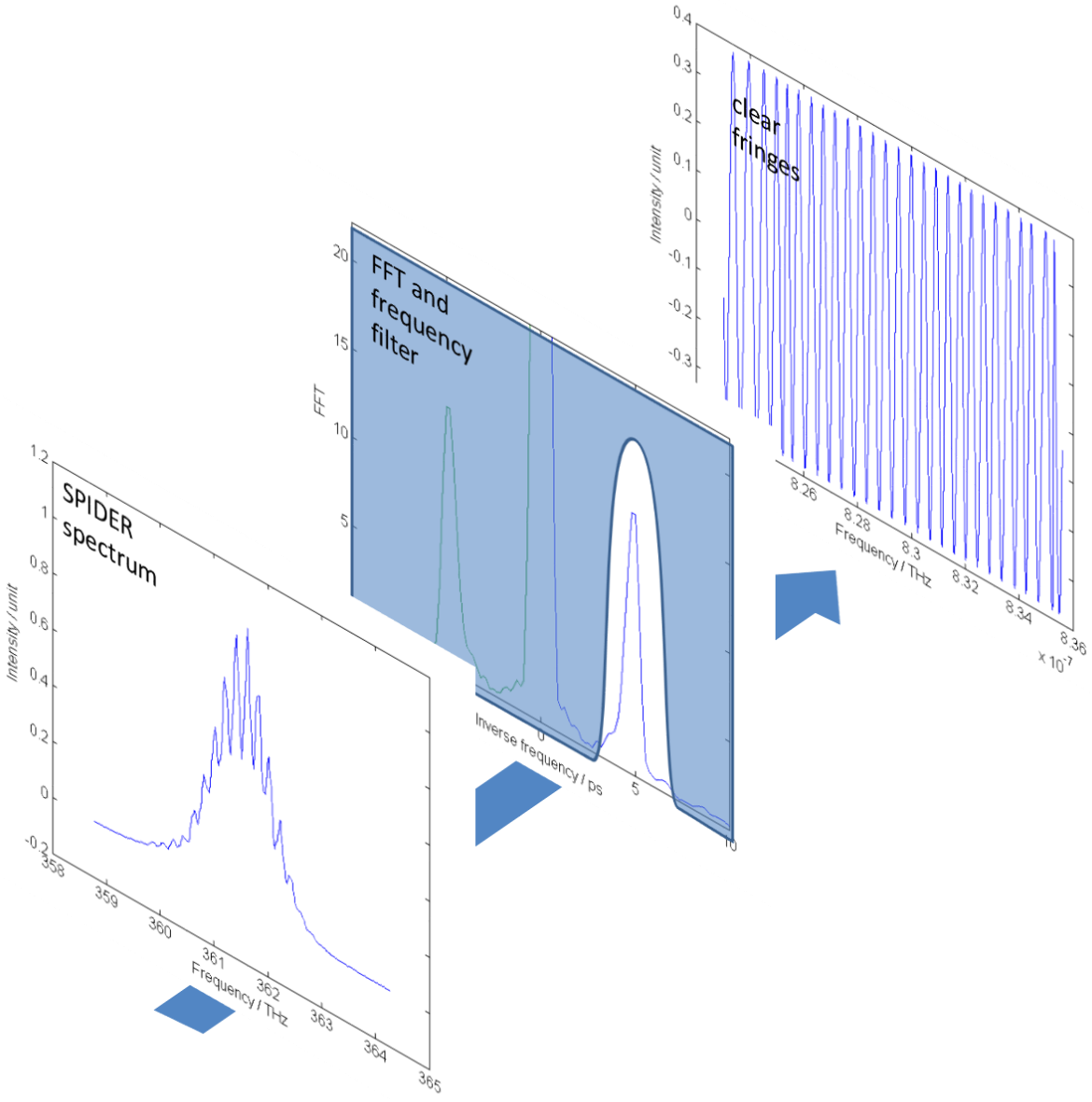

Figure 3-12 Algorithm for obtaining clear fringes

The tricky part is to obtain clear fringes from the spectrum. Shown in Figure 3-12, the interferogram consists of fringes spaced in frequency around $2\pi/\tau$. To retrieve the term $\Phi_D = \phi_\omega(\omega_c-\Omega)-$

$\phi_\omega(\omega_c) - \tau\omega_c$, a common solution is to filter out the unwanted DC component in Fourier space, the $\mathcal{F}(D(\omega_c))$ vs. inversed f. With DC and –AC term filtered out, $D^{AC}(\omega_c)$ is a complex variable and its real team is a sinusoidal wave. The term Φ_D is the angle of the complex value from $D^{AC}(\omega_c)$.

$$\Phi_D(\omega_c) = \arg(D^{AC}(\omega_c))$$

To retrieve ϕ_c, we define phase difference θ,

$$\theta(\omega_c) \equiv \phi_\omega(\omega_c - \Omega) - \phi_\omega(\omega_c) = \Phi_D(\omega_c) + \tau\omega_c$$

and the phase of the spectrum is given by

$$\phi_c(\omega_c) \approx \frac{1}{\Omega}\int d\omega_c \theta(\omega_c)$$

Note that SPIDER technique is only able to tell the second and higher order phase, which corresponds to the chirp of the pulse.

3.4 SPIDER Assembly and Phase Retrieving Procedure

The original optical path for the SPIDER is shown in Figure 3-13. The beam is split at a piece of glass right after it enters the SPIDER. Stretched by the 10-cm-apart grating pair, the transmitted pulse acts as a referencing beam adding the frequency modulation to the pulse replicas. The reflected beam is duplicated at the Michelson interferometer, whose left arm is movable for adjusting the delay. The optical path for the pulse replicas are much longer than the one for the stretched pulse because of the huge group delay in the stretcher. The two beams are focused onto a BBO crystal for SFG.

The CCD of the high resolution spectrometer is no longer compatible with modern PC. Unfortunately, the old desktop is gone, and some files for the old SPIDER program are missing. We decide to connect the spectrometer to an oscilloscope with a GPIB readout, and to rewrite all the programs.

The spectrometer consists of an MS127i imaging spectrograph and a LineSpec detector. The detector is connected to a Tektronix TDS 620B oscilloscope though BNC cables. The OUT port is linked to CH2 and the SYNC port to AUX2. The SYNC port gives a square wave signal as a trigger and the OUT port sends the intensity signal of each CCD pixel. The oscilloscope displays the spectrum in wavelength space and sends data to PC though GPIB communication. The GPIB to USB interface with NI-488.2 protocol is manufactured by National Instruments.

To read the spectrometer and store the spectrum on the computer, a program is implemented in C. The spectrum is stored in the computer on every single shot. Since the trigger to the CCD does nothing, the CCD cannot be synchronized with the laser. As a result the data acquiring efficiency is low. Before the application reads the spectrum, it asks for the file name, the number of shots, and a threshold for recording. The program stores spectrum only when the maximum signal exceeds the threshold.

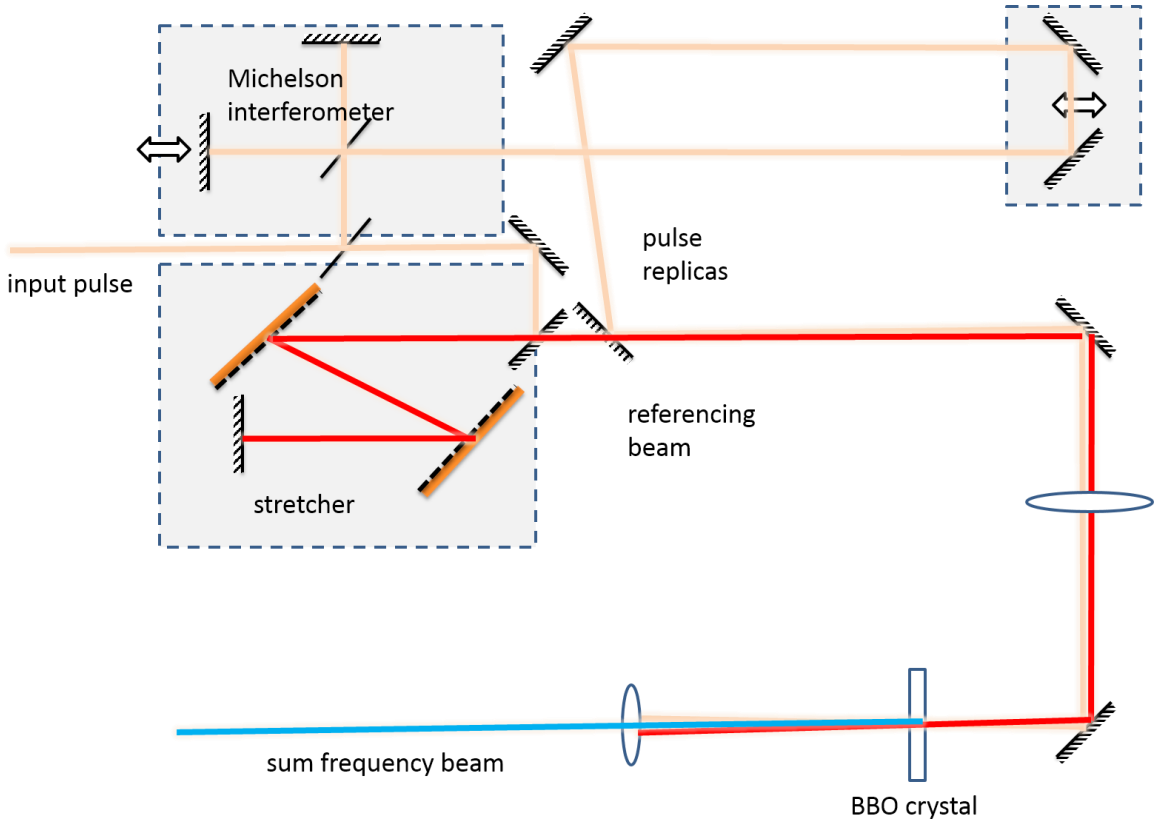

Figure 3-13 The actual optical path for SPIDER

The program for phase retrieving is written in Matlab. The first step is to import the spectrum from a text file. Because of the nature of FFT algorithms, the data points have to have the same interval in x-axis. The second step is to transform the spectrum from wavelength space to frequency space with interpolation to make sure that the frequency interval is the same. Then, filter out unwanted frequency by performing FFT, applying frequency filter, and transforming back. The next step is to compute the angle Φ_D from the complex value. However, the initial Φ_D varies from $-\pi$ to π. The

program then splice it to find the continuous Φ_D. The delay term $\omega\tau$ has to be taken out from Φ_D to obtain phase difference θ. The last step is to integrate the phase difference θ to obtain the phase information $\phi(\omega)$.

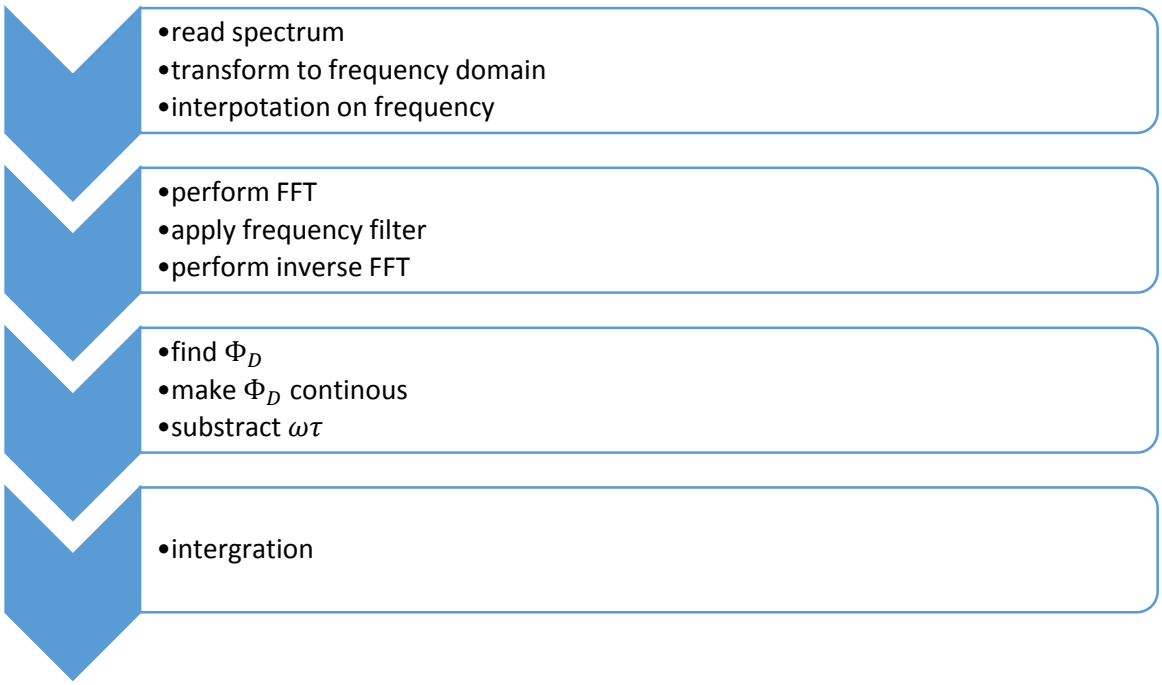

Figure 3-14 Flow char for SPIDER program

4 Measuring Phase Information by the SPIDER

4.1 Modification in SPIDER

Before the phase measurement was started, minor changes were applied to the SPIDER which have been described by James Macpherson in his thesis for characterizing 800 nm 150fs pulses (Macpherson, 2003). During the first experiments with the SPIDER, it was found that the chirped referencing beam is not long enough to provide cross-correlation for two pulse replicas with sufficient separation to see a number of fringes. Thus the FFT filter will not work. Since the bandwidth of the pumps and Raman orders are narrower than it was at the original time, it requires more delay τ to see enough number of fringes than it did. To solve this problem, the space between the two gratings is increased from 10cm to 33cm. Thus, the pulse is stretched 3 times more than before. The optical path for the two-pulse replicas are increased for approximately 80 cm to match the group delay introduced by the extra 23 cm spacing between gratings. Another rotational stage is attached to the crystal mount for easy angle tuning for different frequencies. The optical path for the modified SPIDER is shown in Figure 4-1.

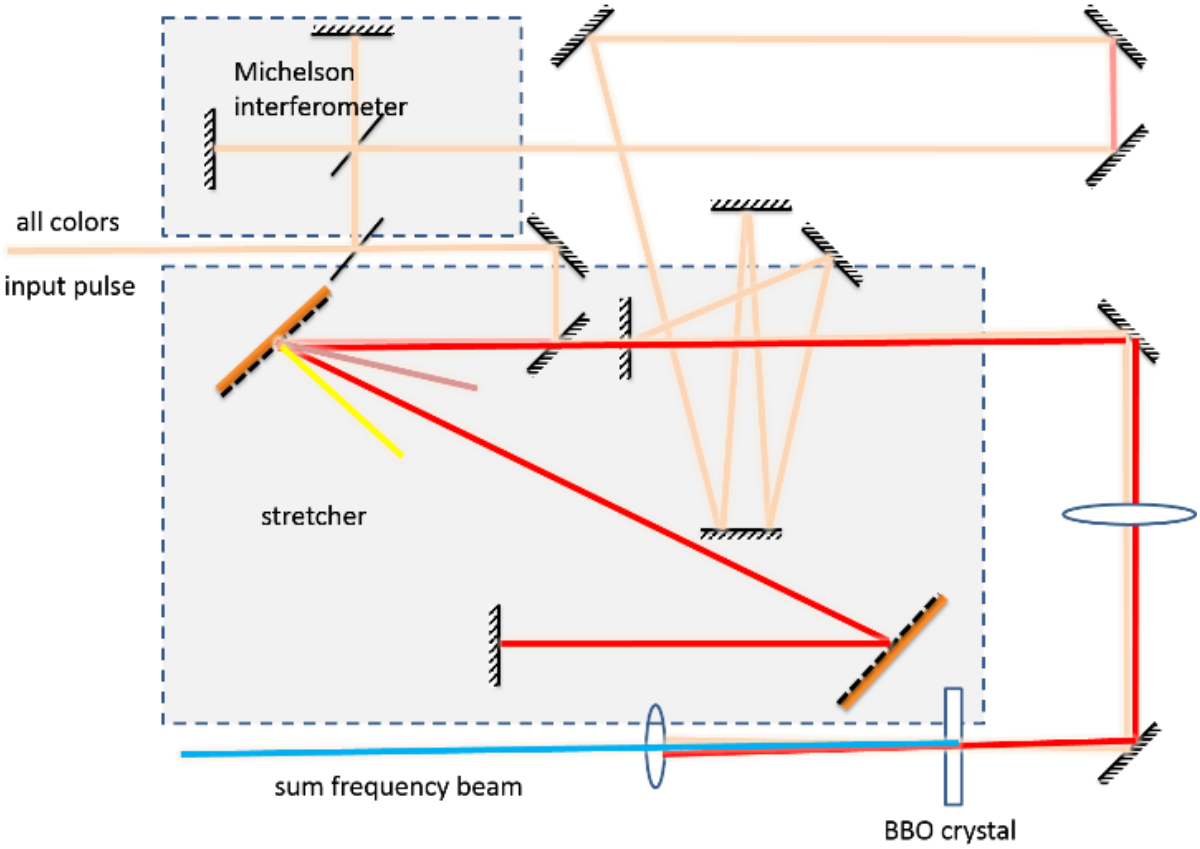

Figure 4-1 The optical path of the modified SPIDER

This setup is capable of performing self-referencing measurements as well as cross-referencing measurement. Due to the nature of MRG produced in the hollow fiber in our lab, the delay between long wavelength pump pulse and other pulses is much smaller (few hundred femtoseconds) than the duration of the stretched referencing beam (15 ps in FWHM), and the diverging angle between different color is small. Switching from one colors to another can be done by simply angle tuning the BBO crystal for appropriate phase matching. The cross-referencing SPIDER measurement was also performed on solid medium MRG where the all colors are not collinearly generated (Matsubara, E. et al, 2009).

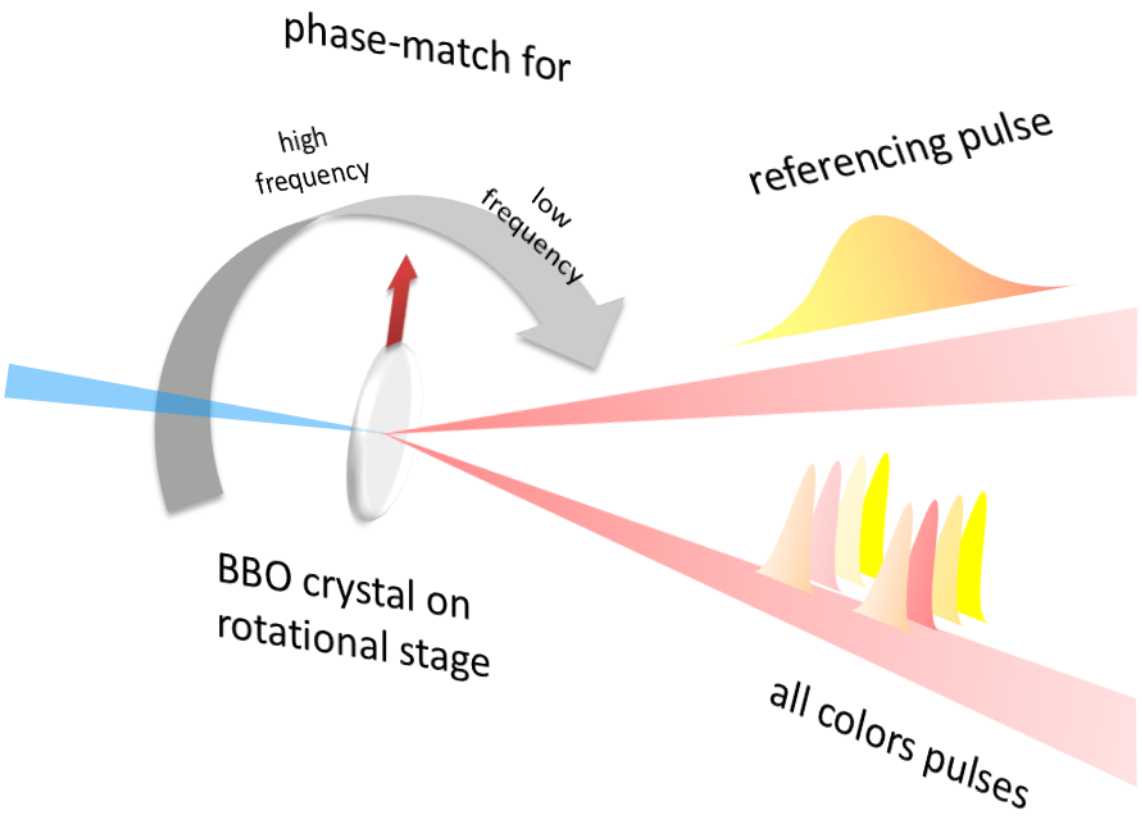

Figure 4-2 SPIDER for pulses with difference frequency

4.2 Calibration of the SPIDER

The spectrometer associated with the SPIDER requires alignment before use. The beam should aim horizontally onto the entrance slit of light for the spectrometer. The final goal for adjusting the spectrometer is to clearly see fringes of the SPIDER. Adjusting the rotation stage for grating can bring the -1st order diffraction light onto the linear CCD. The intensity could be very low if the peak is positioned at some area on the CCD because of some internal alignment issue. It might require tweaking on the front knob to move the focal plane onto the CCD for best resolution if the fringes of the interferometer is blurred.

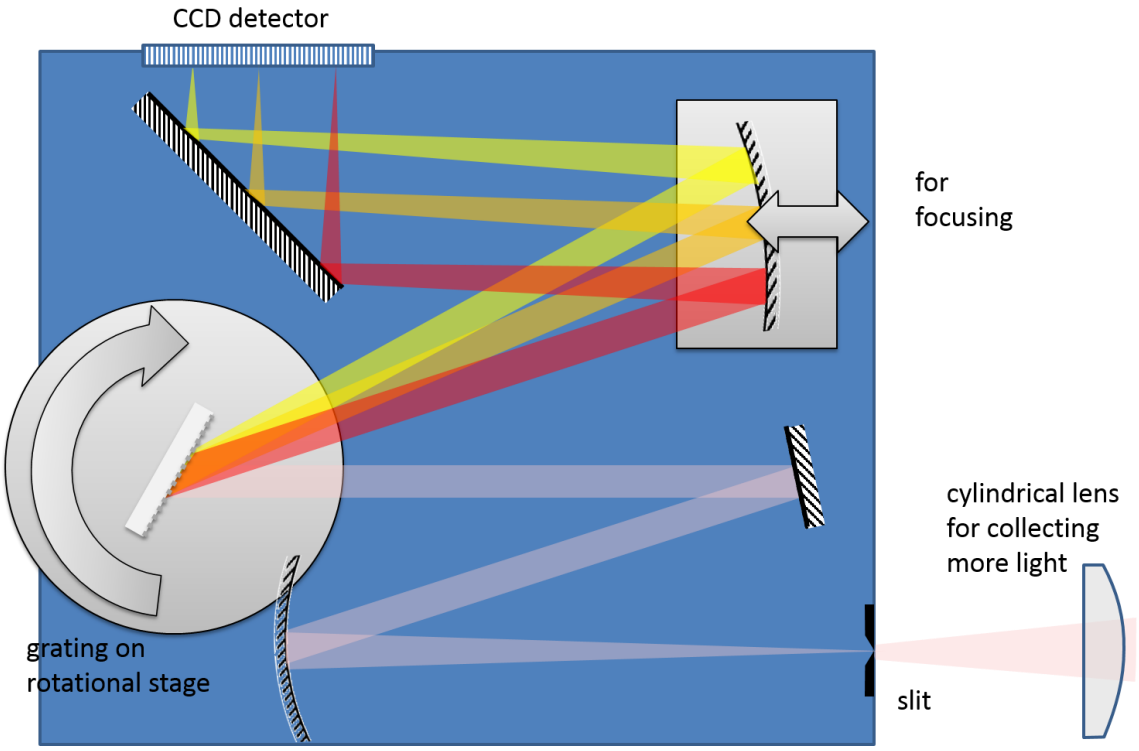

Figure 4-3 The high resolution spectrometer

Since the computer read-out of the SPIDER spectrometer was no longer compatible with our current computers, we had to read the spectrum using an oscilloscope. The output of the spectrometer associated with the SPIDER does not indicate the actual wavelength of the spectrum. We need to find the relation between wavelength and pixels on the oscilloscope connected to the spectrometer. Since the diffraction angle for the grating inside the spectrometer is linear in wavelength space with small incident angle, we can assume that the wavelength is linearly associated with the pixels. Then a two-color calibration is good enough for the spectrometer. To calibrate it, a two-color beam was sent into the spectrometer. Then two spikes are shown on the waveform, and the time t for each spike can be easily read. The value $\Delta\lambda/\Delta t$ is used for calibration since the index of pixel is linear to time t on oscilloscope.

The accuracy of delay between two pulse replicas τ affects the result from SPIDER a lot. It requires recalibration every time when the Michelson interferometer is adjusted. To do this, the spectrum for frequency doubled pulse replicas should be taken, and it should be converted form wavelength

domain to frequency domain. The delay is indicated in the Fourier transform of the spectrum as shown in Figure 4-4. The number of fringes varies on the delay τ, and the change in delay τ has to match the change in the position of the moveable mirror in Michelson interferometer.

The frequency difference Ω is proportional to the delay τ. The relationship between the delay and Ω is calculated based on the GVD equation for gratings in section 2.2. The angle of incidence on grating is $37°$, and the spacing between two gratings is 33cm for a single pass.

If the number of fringes is too small or too large, one should adjust the delay from the translational stage in Michelson interferometer.

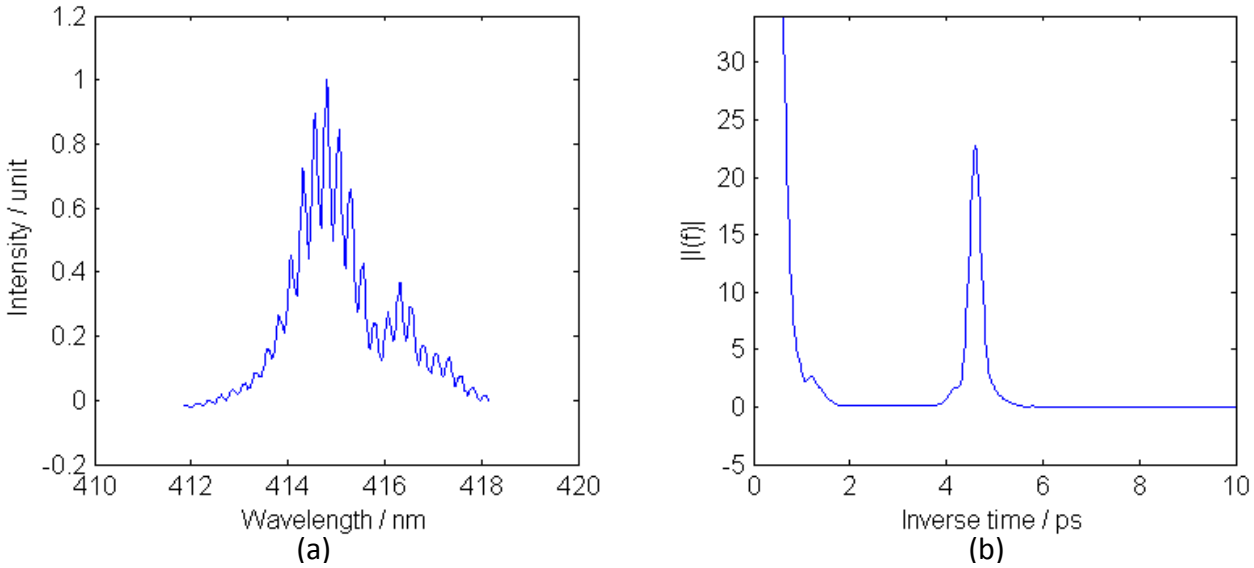

Figure 4-4 The spectrum of the frequency doubled pulse replicas in (a) spectrum domain (b) inverse frequency domain

4.3 SPIDER Reliability

4.3.1 Phase Information Retrieve by Self-Referencing SPIDER

The first experiment is to measure the phase of the positively and negatively chirped pulse to see if the SPIDER is capable to tell the sign of linear chirp of the target pulse. Theoretically one can tell the sign of linear chirp from the Fourier transform of the SPIDER spectrum. In our design, if the FFT peaks at a higher time value than the delay between two pulse replicas, then the linear chirp is negative, but otherwise positive.

To test the self-referencing SPIDER, the regen is producing picosecond pulses at 830nm with 5nm FWHM bandwidth. The wave plate before the SPIDER is rotated to obtain maximum SHG and SFG in the SPIDER. The SPIDER spectra were taken for a 0.6-picosecond positively chirped pulse and then a 0.6-picosecond negatively chirped pulse.

In Figure 4-5, the up-bowled curve is the phase for negatively chirped pulse while the down-bowled for positively chirped pulse. To check the consistency of the data, the phase difference between the two oppositely chirped pulses is compared with the phase change provided by a grating pair separated by approximately 4 cm.

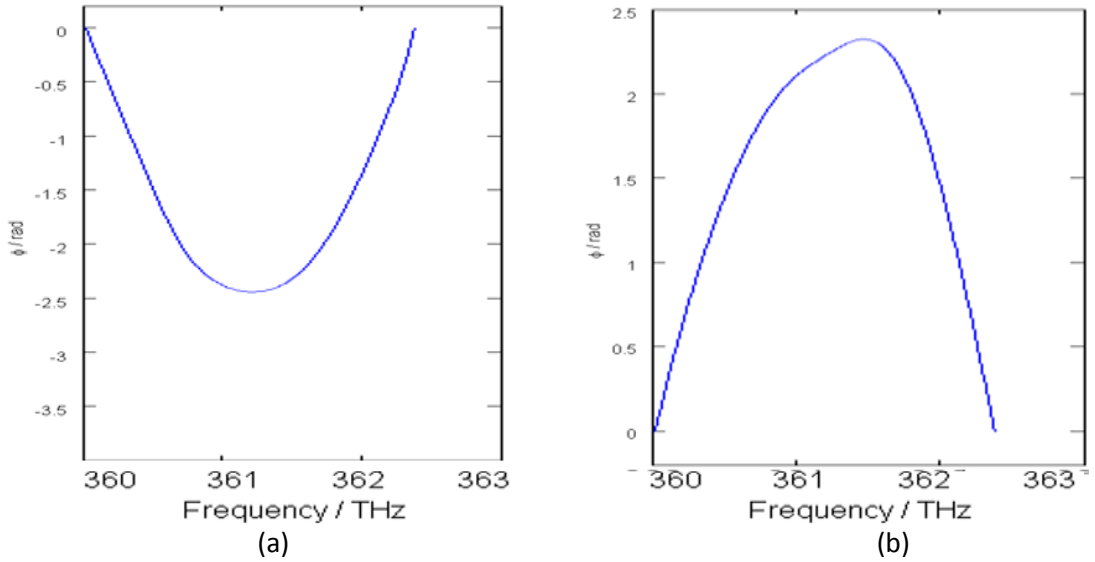

Figure 4-5 Phase of a (a) negatively chirped pulse (b) positively chirped pulse

4.3.2 Phase Measurement by Cross-Referencing SPIDER

To measure the phase other than the long wavelength pulses (centered on 830nm), we decide not to use self-referencing SPIDER for the following reasons. There is an option to use cross-referencing SPIDER for different colors. Switching between different colors is as easy as tweaking the BBO crystal when all colors are roughly timed up.

One the other hand, if we do self-referencing SPIDER for all colors, it requires a huge amount of work to build optical paths for different referencing beams because those colors are diffracted in different angles at the gratings and a lot of effort to compensate the various group delay for all different colors.

We performed the phase measurement on the beams from the 1st anti-Stokes Raman orders to the 1st Stokes Raman orders. Though the blue light generation for Raman orders is weak, we can boost the energy going into the spectrometer by placing a cylindrical lens to focus the beam at its entrance slit. As expected, the Raman orders are chirped with same sign as the pump pulses. The spectra and relative phase curves are of each colors are shown in Figure 4-6. The bandwidth of the SPIDER spectrum is narrower than the original spectrum. As a result, the spectrum cannot be retrieved from

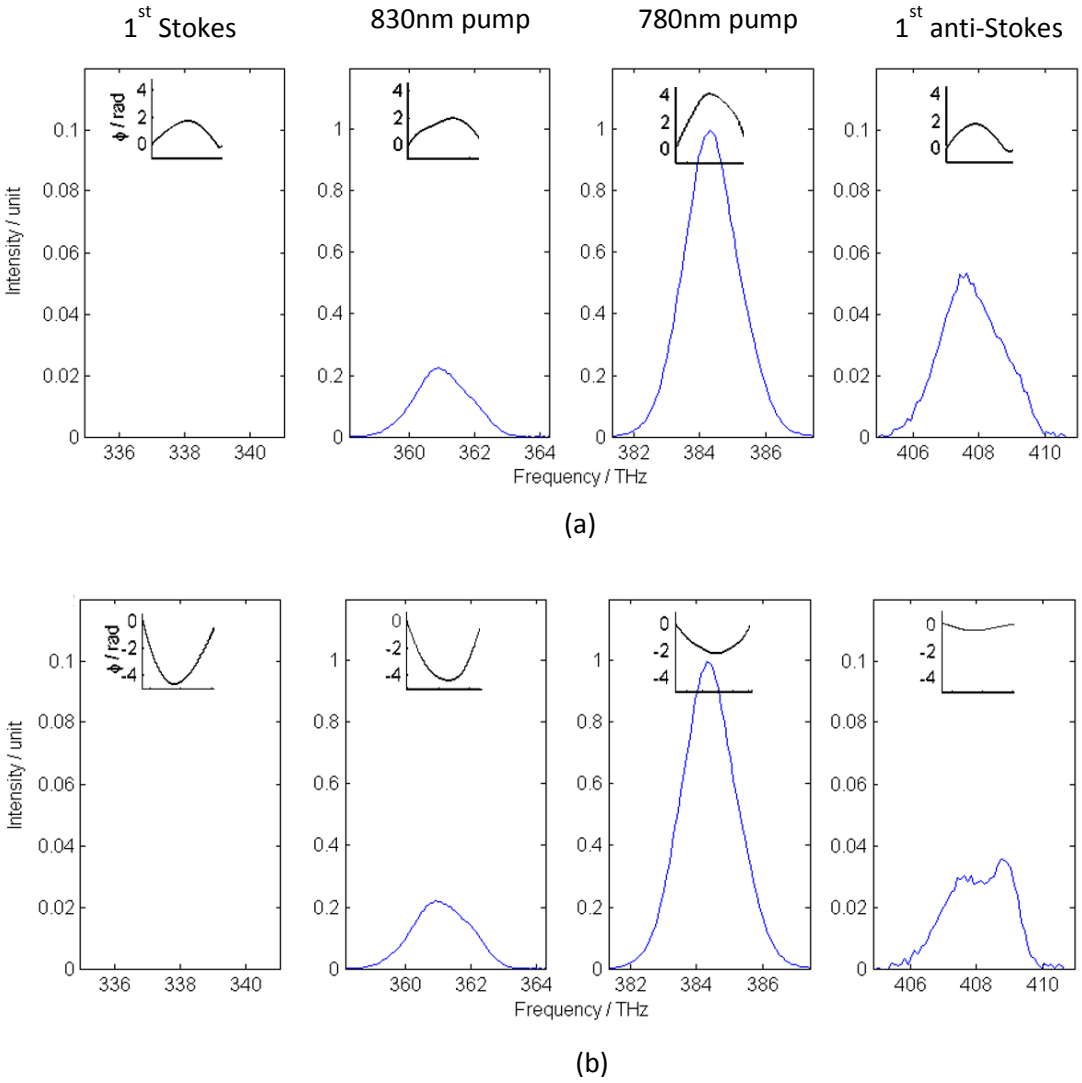

Figure 4-6 Spectrum (blue lines) and phase (black lines) of pumps and Raman sidebands with (a) positively chirped pumps (b) negatively chirped pumps

the SPIDER and the phase measurement is inaccurate at the wings of each color. The spectrum is taken from a broadband spectrometer. We only take the phase near the central frequency of each

color, where the SPIDER spectrum has clear fringes. The spectrum of the first Stokes order is not measured because our spectrometer does not work at that wavelength.

The SPIDER was initially designed for measuring an 800 nm infrared laser. IR dielectric mirrors were chosen at that time, resulting now in significant energy loss for the short wavelength Raman components. Blue light generation for the 2nd anti-Stokes Raman order and above is hardly detectable at this time.

4.3.3 Accuracy of the SPIDER

In this section, the accuracy of the SPIDER is discussed. We are more interested in how the phase curve changes in different configuration than what the absolute phase curve is. Once the measurement is started, all calibration values are fixed and every measurement has similar error caused by imprecise calibration. Thus, small error from calibration will not be a concern. A few measurements has been taken to check if the SPIDER has satisfying accuracy.

The result from SPIDER should be independent on the delay τ. This is the first accuracy check. Figure 4-7 shows phase curves of 5 different measurement. Trial-1 and 2 are exactly of the same condition of the SPIDER. Before trial-3 is taken, the translational stage in the Michelson interferometer is moved forward for $225\mu m$. Trial-4 is taken when the translational stage is set back as trial-1. Finally, the stage is moved forward again for $120\mu m$. The difference between the highest and lowest curve is 5% consisting error from calibration and random noise, and the fact that the laser itself is changing.

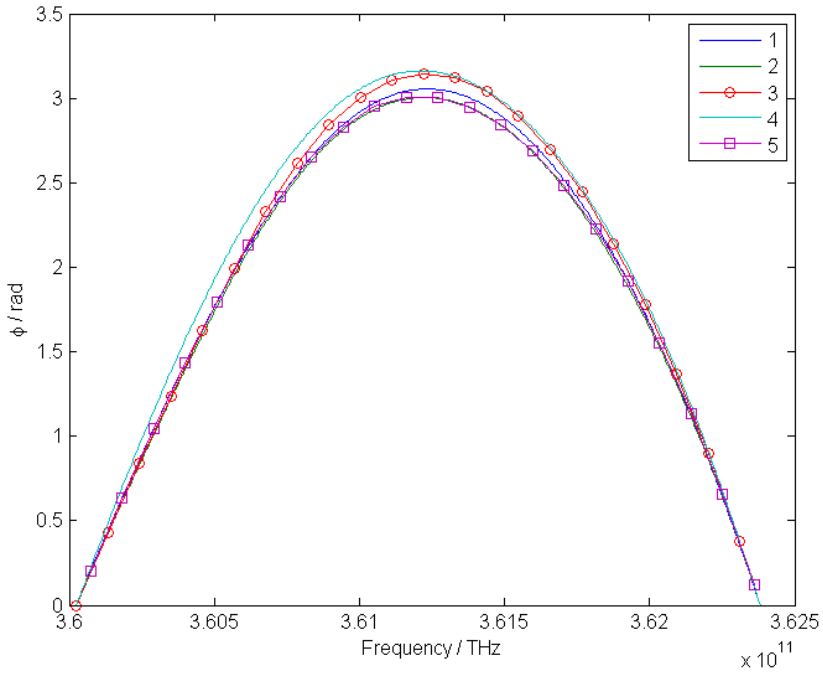

Figure 4-7 The phase curve measured with different delay

The second test is to compare the measured phase of the pulse to the computed value for different grating separations. Unfortunately, finding a position of the grating with flat phase is impossible since the system has significant 3rd order dispersion that cannot be completely compensate by the grating compressor. Alternatively, the simulated phase is compared to the change in phase brought about by a specific separation change in gratings. Shown in Figure 4-8, the phase is measured when the grating is moved backward for 6.4 and 10cm and the phase at the reference position is measured three times during the whole experiment. The experimental results match the expectation very well with error less than 10%.

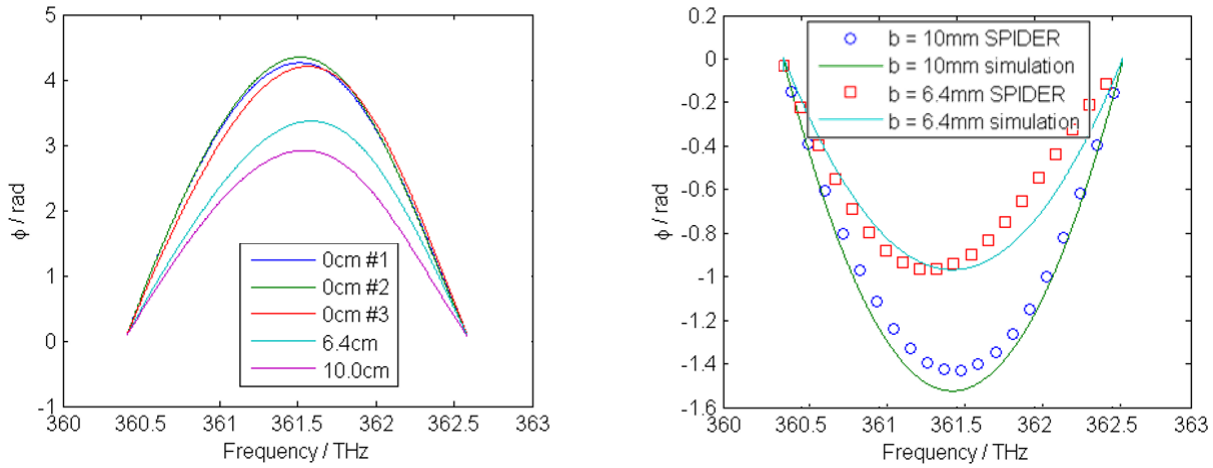

(a) (b)

Figure 4-8 (a) phase of the pulse with various separation of gratings (b) comparison between measured phase difference and estimate

Theoretically, the accuracy of the SPIDER is independent on the intensity of the pulse. However, a strong pulse will saturate the spectrometer for sure. This can be avoided by placing a filter right before the spectrometer to decrease the energy going through. Figure 4-9 shows the measured phase with same configuration except for placing a glass filter or not before the spectrometer.

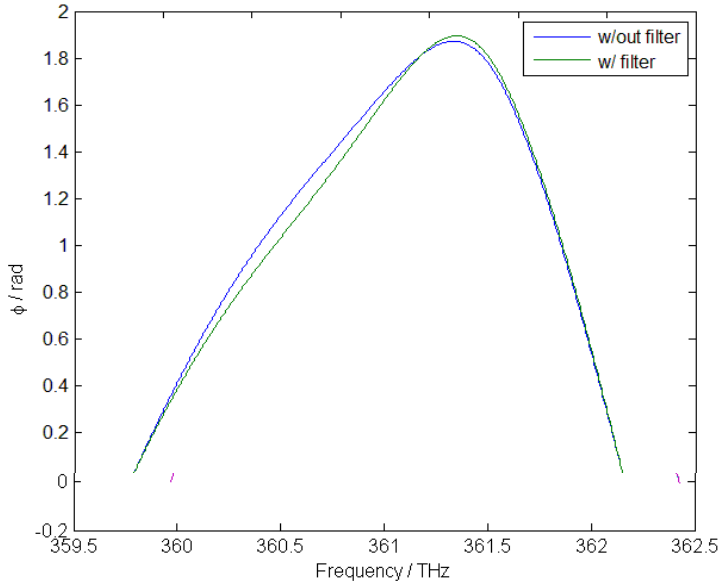

Figure 4-9 measured phase with and without a filter before spectrometer

4.3.4 Pulse Compression by Prisms Checked by SPIDER

Pulse compression of the pump pulses after the hollow fiber using a prism pair was done previously in the lab. Compression measurements at that time were done by auto-correlation (Yan, 2011). Two types of prisms were available in the lab for the compression experiment, SF14 and LK21. SF14 prisms have more GVD than LK21 prisms with the same spacing. With the SPIDER, we can measure the change in GVD before and after the prisms pair. The result would be useful for compression of Raman orders in the future.

For pulse compression, SF14 prisms are chosen due to the higher compression efficiency. This pulse compressor is shown in Figure 4-10. Due to the limited space on the table, the optical path is folded by a rectangular gold mirror. The separation between two prisms is 350 cm. Back mirrors are mounted on translational stages for timing except the 830nm beam. All prisms are mounted on translational stages for alignment. The double prism design is used because the height of a single prism is too small to separate the in and out beam vertically.

Cross-correlation experiments are performed with the short wavelength pulse and long wavelength pulse after the prism compressor. The timing of the pulses can be confirmed by cross-correlation. It should be noticed that moving the translational stage for the second prism will bring multiple picosecond delay between two pulses. The optics should be mounted on stable bases to reduce misalignment over time. Pinholes should be placed before and after the first prism for better reproducibility.

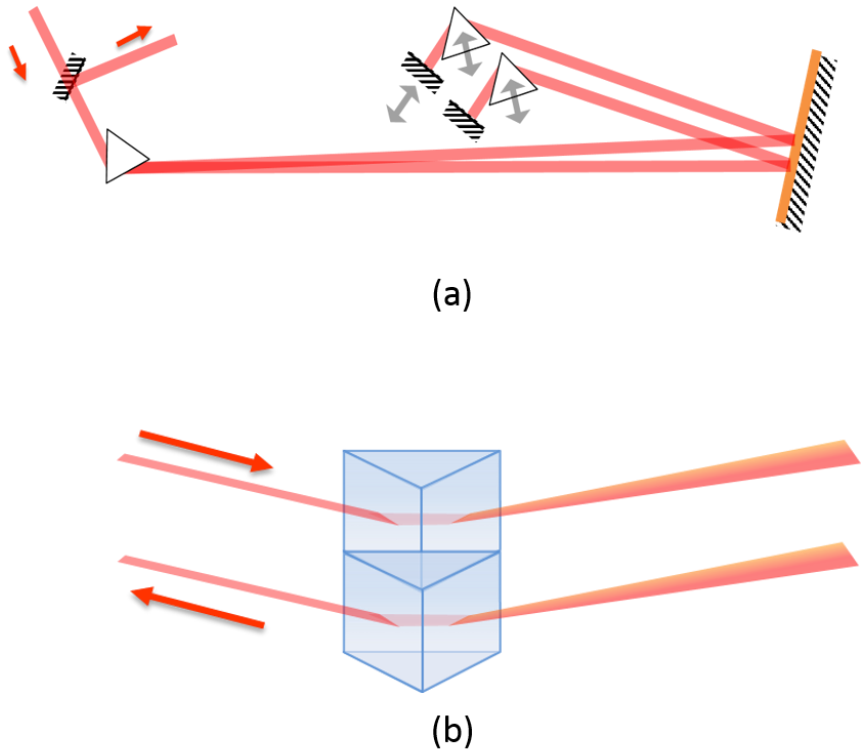

Figure 4-10 The prism pair compressor set-up

A simple pulse compression experiment is performed on the 830nm beam. While the pulse after the prism compressor is being auto-correlated, we move the grating in the CPA compressor back and forth to find a position that gives a pulse as short as possible. Then, as shown in Figure 4-11, the phase of the input and output pulses of the prism compressor are compared. The difference makes a quadratic line as expected.

Though the polarization of the beam is adjusted to minimize the reflection on the surface of the prism, there is still 50% energy loss though the compressor.

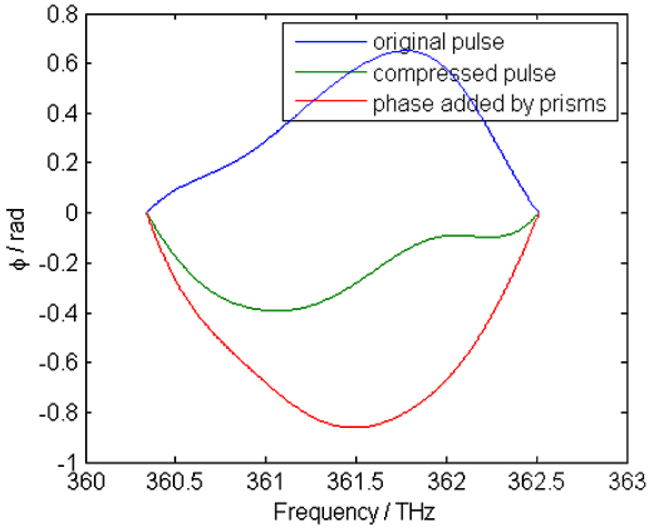

Figure 4-11 The phase of the 830 pump pulse changed by prisms

5 Noise and Drift in Laser System

This chapter is focused on noise treatment for the SPIDER measurement. Noise in the laser system is a factor that may have great impact on the result. There is a 10% fluctuation in the energy of the green pump pulse since the reproduction rate is only 10 Hz resulting in varying output power from the regen. Moreover, unstable air current affects the stability of the regen a lot. Besides, the ultra-short pulses may experience SPM, which is highly related to energy per pulse, in the some optical components. As a consequence, the auto-correlation trace is of 10% to 20% uncertainty, and the spectrum of the laser is varying from shot to shot.

There are several ways to reduce the error from a system with noise. A passive solution is to take as many measurements as possible and average the result. However, 1000 measurements on phase takes a long time because of the low repetition rate of the laser and the performance of the spectrometer. The temporal drift of our laser is the main concern when the measurement is running for too long. Thus the problem cannot be solved by simply increasing the sample size. Another approach is to find the source of noise and to reduce the noise in the system. The fiber delivering the seed pulses to our lab was considered to be the main source of noise. A few changes have been made on how to transmit the seed pulses to our CPA.

5.1 Noise Treatment

The common solution for increasing precision of noisy system is averaging multiple measurements. However, it brings the question 'do we apply averaging for the SPIDER spectrum or the retrieved phase'. There is no simple answer for it. Figure 5-1 shows the averaged SPIDER spectrum with 300 shots. In a very noisy system, the density of fringes is changing, leaving a highly blurred averaged spectrum. However, a single shot spectrum is more likely to be with random micro structures that cannot be corrected by FFT filter than an averaged spectrum. Those structures will result in inaccuracy. If the phase curve of the target system is stable, the averaged fringes will be clear and free from random noise on the envelope of the fringes. Averaging before retrieving the phase consumes little time as the program only call the SPIDER function once. In conclusion, if the averaged spectrum is not blurred, it is recommended to average the spectrum before retrieving the phase.

Otherwise, one should run the SPIDER program for every single shot and then average the phase curve

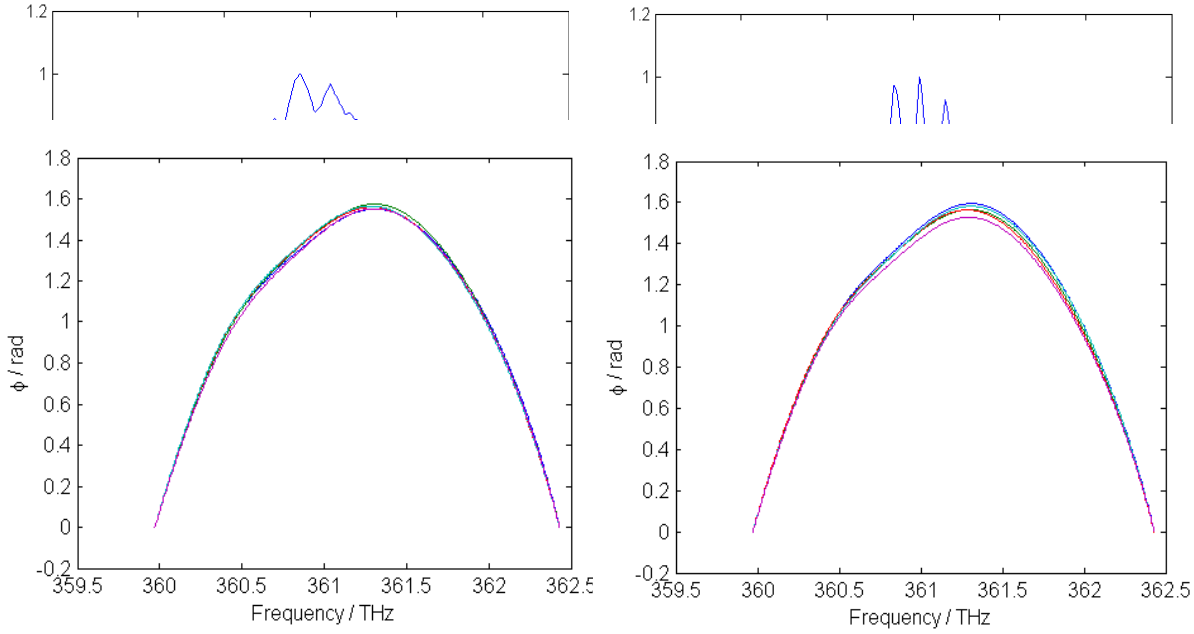

Figure 5-2 Random error of (a) phase retrieved from averages spectrum (b) averaged phase retrieved from single shot spectrum

In Figure 5-2, a comparison of the different configurations is shown. In (a), the phase is retrieved from an averaged SPIDER spectrum, while in (b), the phased is retrieved first, and then averaged. Each line in both figures is with 200 sample size. To avoid temporal drift, we chose the 1^{st}, 5^{th}, 9^{th} shot and so on for the first line, 2^{nd} ,6^{th}, 10^{th} shot and so on for the second, and similarly for the following 3 lines in each figure. The random noise is slightly smaller if the spectrum is averaged first before calculating the phase in this case. However, if the phase is varying very much from shot to shot, the averaged spectrum would give unreasonable phase since the fringes are blurred.

We thought that some of the noise was from SPM in the fiber. A second 5cm-long water cell is placed before the fiber to further stretch the seed pulses. Thus, the nonlinear effects that adds instability to the phase, such as SPM can be reduced. In Figure 5-3, both plots are the averaged single shot phase. The only difference between the two plots is that (b) is taken with a water cell before the fiber in place. However, there is not much improvement.

5.2 Modification in Seeding the CPA System

Even though the water cell did not improve the noise, we still assumed that the unstable output was caused by the self-phase modulation process in the fiber because of fiber misalignment and the temperature dependence of the refractive index in the fiber and the changing environment lead to the temporal drift.

Our second trial was to discard the fiber set-up, but sent the seed beam through the air to our pulse stretcher. After several measurements, we decided to keep that change. The beam is raised by a parascope from the table level to go through the hole in the wall, and then lowered down by another one to table level in Dr. Strickland's lab. Though the two tables in the different labs vibrate asynchronously, the position of the beam is stable compared to the beam size. Examined by a CCD

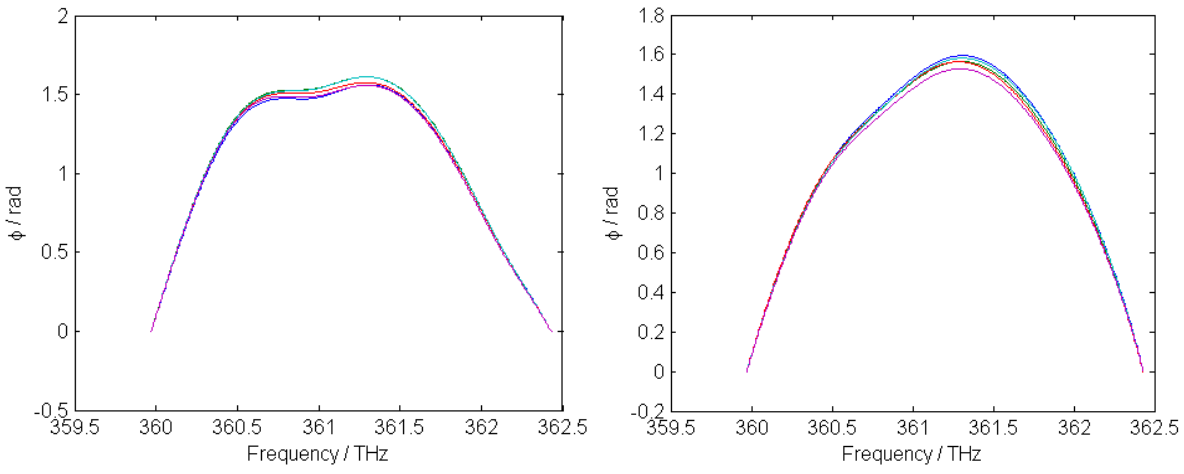

(a) (b)

Figure 5-3 Random phase error of pulses seeded (a) without water cell before fiber (b) with water cell before fiber

camera, the center of beam spot is moving within a distance which is 10% of its diameter. Due to the large divergence in the seed beam, a 5:1 telescope is added into the optical path to reduce the beam size. A half wave plate is placed before the first Faraday isolator to maximize the energy going through.

The absolute and relative random error is smaller than before.

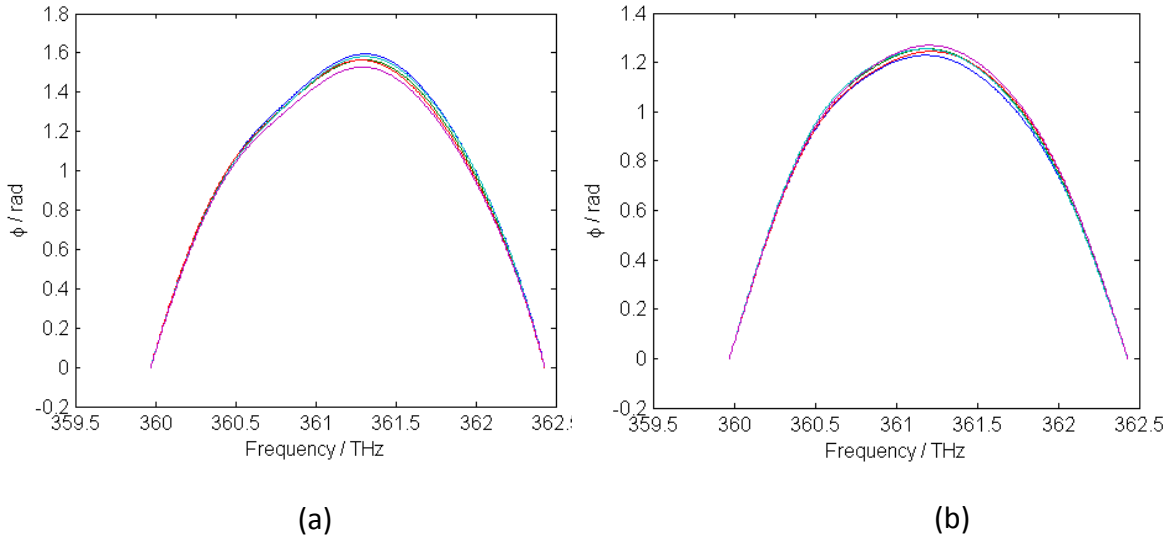

(a) (b)

Figure 5-4 Random phase error of pulses when seeding beam propagates (a) in fiber with water cell (b) through air

5.3 Temporal Drift of the Phase Information

The temporal drift of the phase is shown in Figure 5-5. The interval between each trial is 15 minutes, and each trial contains 300 shots. The temporal drift is more than random noise. It was the major problem in our system. Unfortunately, the temporal drift is still not predictable. The direction and speed of how it is changing is random and so affected the other experiments. That brought a lot of difficulties for the study. Sometimes, it seems to be that the drift had been greatly reduced, but the result shows huge error because of the drift. A suggestion is to optimize the data acquiring process to improve the sampling rate. Then, the measurement will take less time and have less effect from the temporal drift.

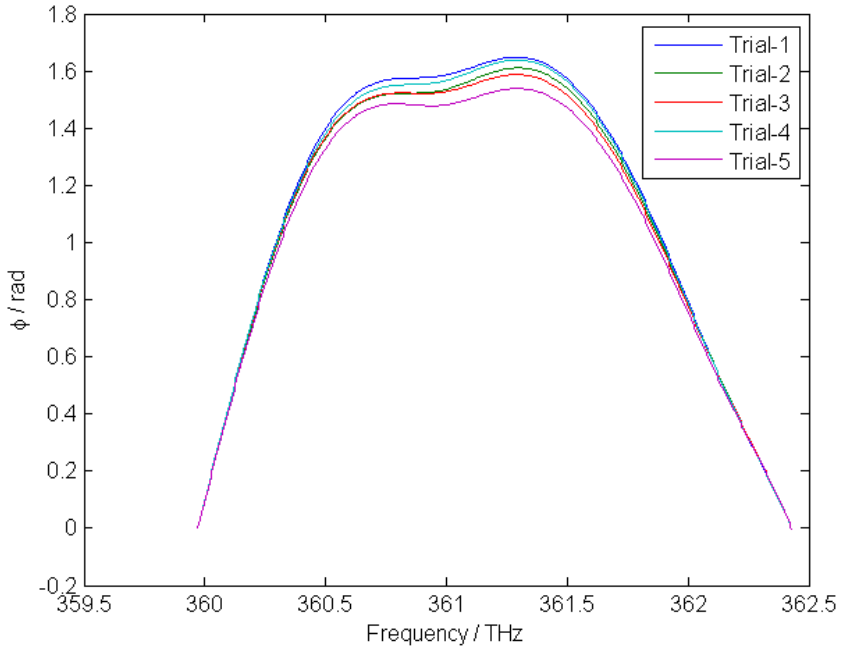

Figure 5-5 Temporal drift of the phase

6 SPIDER Measurements Related to MRG

The GVD inside the fiber is another interest of study. A mathematical model with different inner diameter of the hollow fiber has been developed by Turner in his thesis (Turner, 2006). Lots of measurements had been taken to determine if we could calculate the GVD by measuring the phase before and after the fiber for the pump pulses and the Raman orders. It turns out that the difference in phase was too small so that it is overwhelmed by the high noise and drift.

6.1 Phase vs. Pressure in Hollow Fiber

To determine if the phase difference could be larger than the drift, different measurements under the same conditions have been taken. The two different measurements are shown in Figure 6-1 (a) and (b) where the pressure in psi stands for the value above 1 atm. There are 1000 shots taken for each pressure and it takes 1 hour to complete one pressure configuration. However, the two measurements give totally different results. Looking at each pressure, it is found that the drift and noise is too large. The data of 10psi in trail 1 is divided into 4 parts and each line stands for 15 minutes. The 4 parts are plotted in (c). The same operation is performed for trial 2 and the result is shown in (d). That drift is so much that the fringes for 10psi is blurred and the phase cannot be retrieved correctly.

Similar experiments were performed several times. Unfortunately, the drift was always too large. Further study should be taken only when the sampling rate is increased, otherwise the measurement would be too slow and the experiment would end-up just measuring the drift.

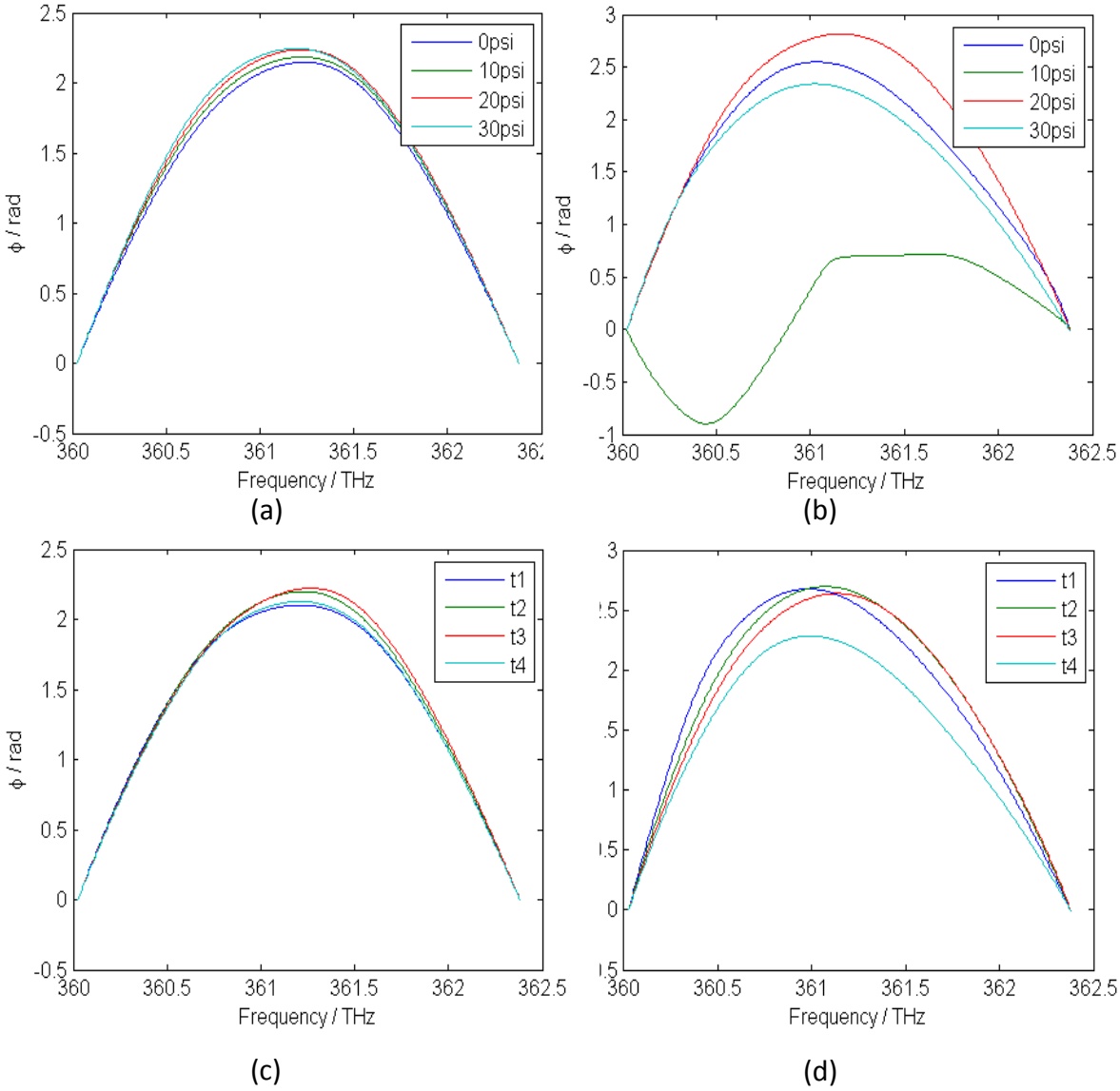

Figure 6-1 The phase curve with pressure change. (a) trial 1 (b) trial 2 (c) temporal drift for 10 psi in trial 1 (d) temporal drift for 10 psi in trial 2

6.2 Timing Dependency of MRG

This study of transient regime MRG is to characterize the phase of the Raman orders for pulse compression in the future, as well as to understand the MRG process with more details. Using two chirped pump pulses for MRG provides the opportunity to study the effects on MRG by different frequency detuning. It had been found in our lab that by red-detuning the MRG process, the Raman orders are red-shifted and spectral broadening occurs. This previous research showed spectral broadening occurs only with red frequency detuning in the two pumps. The asymmetry brings about the question of whether there are other processes that we have not included in our MRG model. On the other hand, a broader spectrum has more potential for pulse compression. It is important to know what the chirp of the broadened Raman order is for pulse compression. It is interesting to see how the chirp of the Raman order changes with detuning of the pumps. This section will focus on the change in phase curve with frequency detuning.

6.2.1 Spectrum of MRG with Frequency Detuning

The two pumps are centered at 830 and 780 nm with 4nm bandwidth. The short wavelength pump pulse is chirped to 900 fs either positively or negatively and the phase of long wavelength pump is matched to the former. Figure 6-2 is the spectrum of the pump in frequency domain. The following Figure 6-3 shows the spectrum of 1st and 2nd anti-Stokes orders with positively chirped pumps and negatively chirped pumps. In both situation, red-shifting occurs with red-detuning.

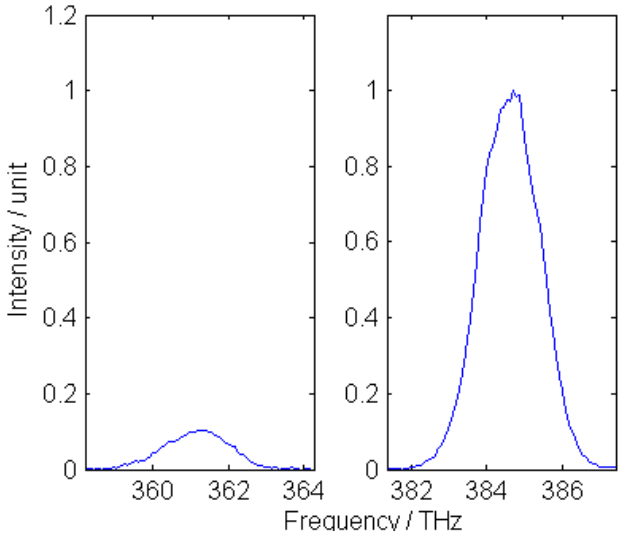

Figure 6-2 The spectrum of MRG pumps

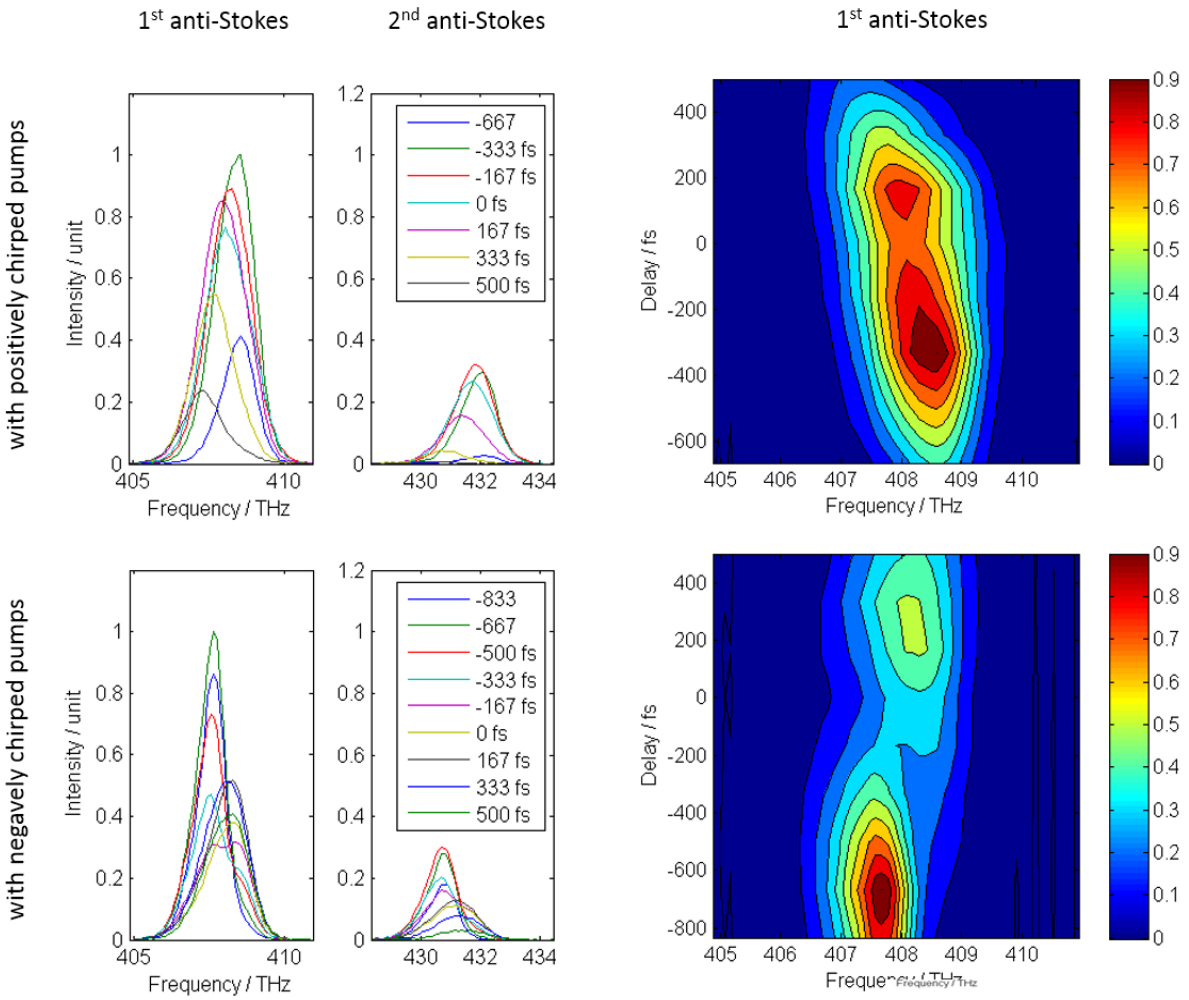

Figure 6-3 The spectrum of the 1st and 2nd anti-Stokes Raman orders with detuning

It is our curiosity to see if oppositely chirped pumps induce MRG and if there is any shifting in frequency. The short wavelength pump pulse is negatively chirped and the long wavelength pump pulse is positively chirped. Surprisingly, the MRG still exists though the instantaneous frequency difference is changing fast from the pulse front to the end in this situation. The spectrum is shown in Figure 6-4 without significant frequency shifting.

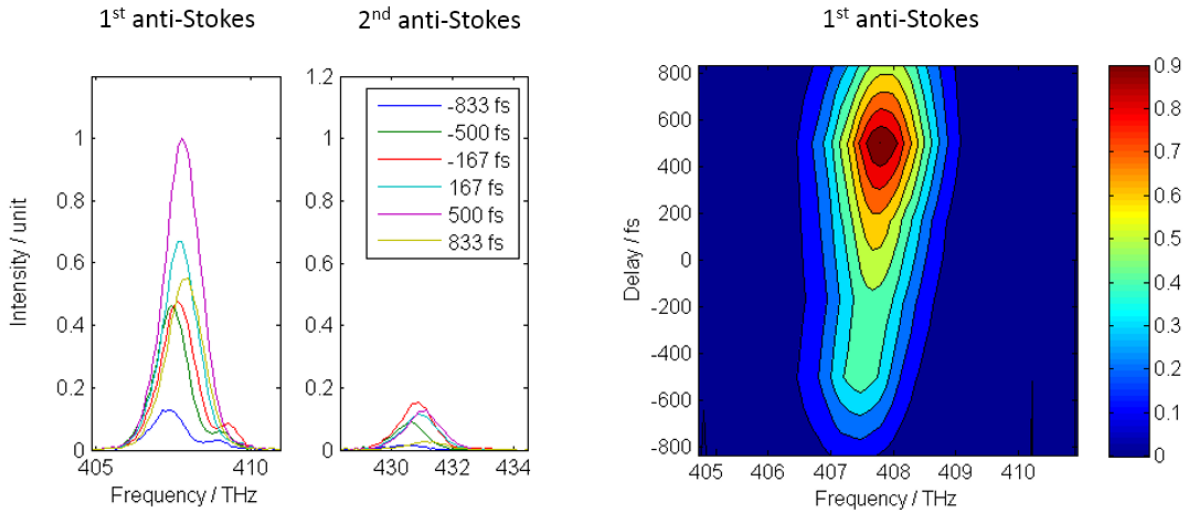

Figure 6-4 The spectrum of the 1st and 2nd anti-Stokes Raman orders from oppositely chirped pumps with detuning

6.2.2 Phase Information of MRG with Frequency Detuning

In Figure 6-5, the phase for the pumps and the 1st anti-stokes orders are shown with varying timing. At first it appeared that more positive chirp is introduced with more red-detuning and then this process stops at large detuning. However, from the consistency check, the temporal drift is towards the more positive chirp direction. There is still the same trend that more red-detuning and more positive chirp. Data on different day are not very coincident. Sometimes the trend on how the phase is changing is completely disordered. The MRG process might be of high nonlinearity that slightly change in chirp and intensity of the pump pulses would result in huge change in the Raman orders.

The Experiment with negative chirped pulse is of low accuracy. The reason is that with the same delay in SPIDER, the number of fringe for a negatively chirped pulse is less than the one for a positively chirped pulse. Thus, the FFT process cannot filter out the structures of the envelope of the spectrum from the fringes because they have similar frequency. As a result, the retrieved phase is affected.

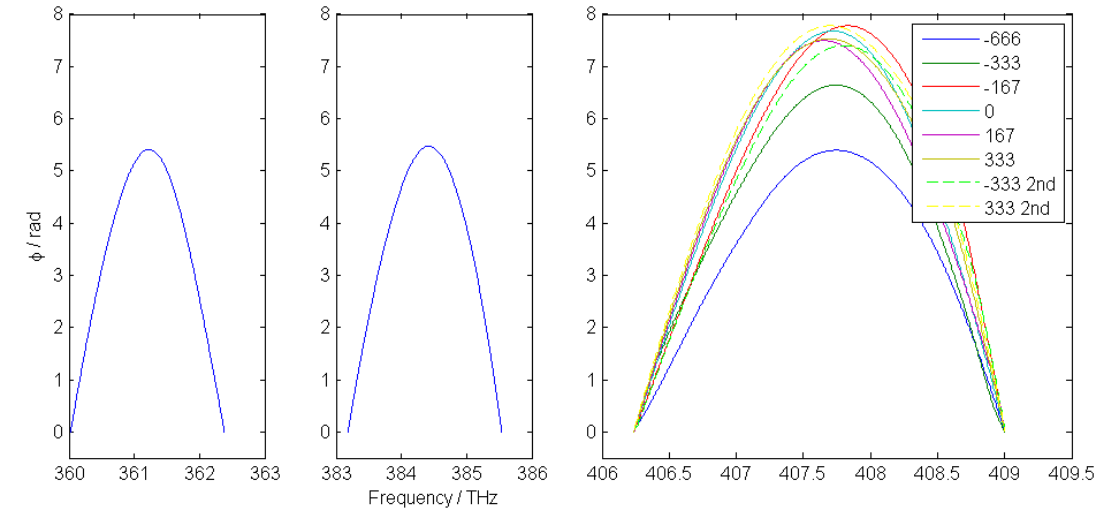

(a)

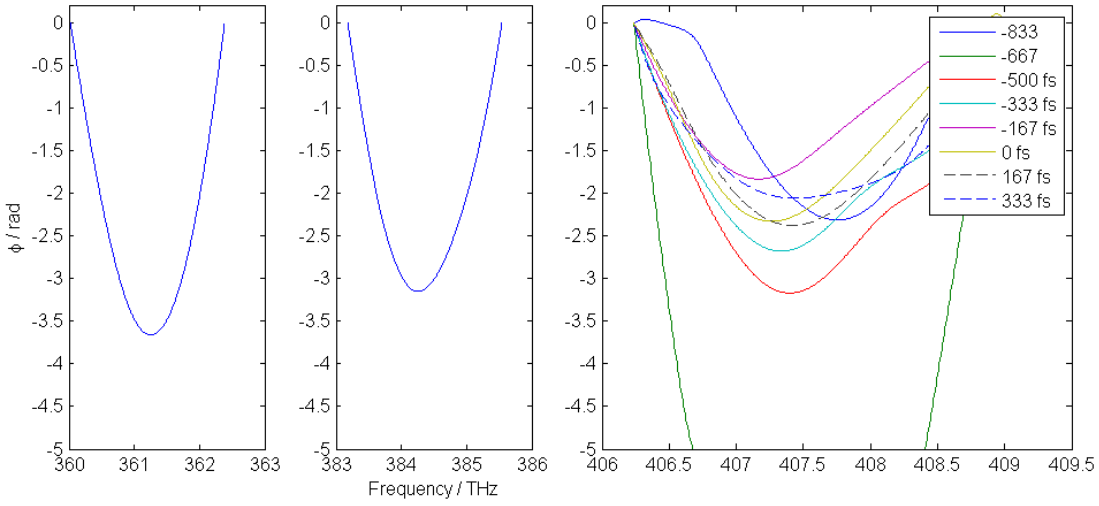

(b)

Figure 6-5 The phase of 1st anti-Stokes Raman order with detuning from (a) positively chirped pumps (b) negatively chirped pumps

Here is another set of data shows the same trend as the first one with positively chirped pulse in Figure 6-6.

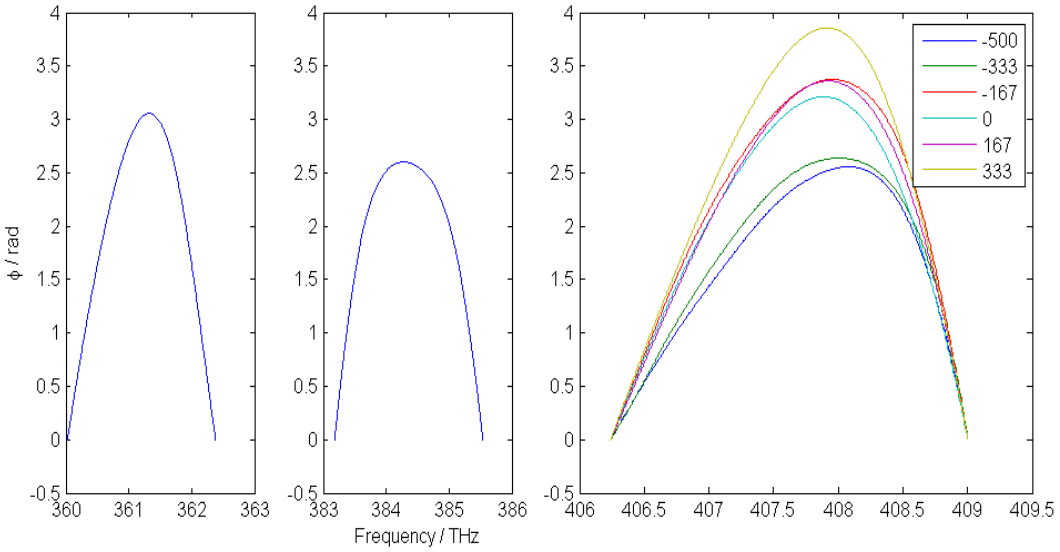

Figure 6-6 The phase of 1st anti-Stokes Raman order with detuning from positively chirped pumps

7 Discussion

Temporal drift is the main concern of the SPIDER measurement. Although the fiber was considered to be to the main reason for temporal drift and so is now removed from the CPA laser, the drift is still too large for the pressure and detuning study. The laser stability and SPIDER efficiency needs improvement as well as the methodology could be changed. After removing the fiber after the mode-lock oscillator, the random noise in the CPA is reduced. The whole experiment could be divided into a few short experiments to reduce the change brought by drift and repeated for a few times.

8 Concluding Comments

The old SPIDER is adapted to our current laser. It gives satisfying result and the error is within 10%. It is able to perform self-referencing measurement on 830 nm pulses, and cross-referencing measurement on pulses from 735nm to 886 nm with the presence of 830nm pulse. To measure the pulses with wavelength below 735, all IR mirrors should be replaced by broad band mirrors except the two in pulse stretcher. The GVD dependency on pressure in fiber shows that the GVD change is below the laser drift level. The chirp of 1st anti-Stokes Raman order might be indicating that when the pumps are positively chirped, red-detuning brings more positive chirp. However, the SPIDER needs improvement on data acquiring rate to reduce the effect from temporal drift.

References

Aussenegg, J. A. (1983). Collinear and Noncollinear Emission of Anti-Stokes and Second Orders Stokes Raman Radiation. *Optics Communications 37*, 59-66.

Boyd, R. W. (2008). *Nonlinear Optics, Third Edition.* Academic Press.

Cui, Z. and Strickland, D. et al. (2013). Spectral red-shifting of multi-frequency Raman orders. *Optics Communications 288 1*, 118-121.

Iaconis, C. and Walmsley, I. (1998). Spectral phase interferometry for direct electric-field reconstruction of ultrashort optical pulses. *Optical Letters 23 10*, 792-794.

Imasaka, T., Kawasaki, S. and Ishibashi, N. . (1989). Generation of more than 40 laser emission lines from the ultraviolet to the visible regions by two-color stimulated raman effect. *Applied Physics B 49*, 389-392.

Losev, L. L. et al. (2002). Multifrequency parametric infrared Raman generation in KGd(WO4)2 crystal with biharmonic ultrashort-pulse pumping. *Optics Letters 27*, 23.

Macpherson, J. B. (2003). *Characterisation and Optimazation of Ultrashort Laser Pulses.* Waterloo.

Marcatili, E. and Schmeltzer, R. (1964). Hollow Metallic and Dielectric Wave-guide for Long Distance Optical Transmission and Lasers. *Bell System Technical Journal 43*, 1783-1809.

Matsubara, E. et al. (2009). Generation of ultrashort optical pulses in the 10 fs regime using multicolor Raman sidebands in KTaO3. *Optics Letters 34 12*, 1837-1839.

Shigetaka Yoshikawa, Totaro Imasaka. (1993). A new approach for the generation of ultrashort optical pulses. *Optics Communications*, Volume 96, Issues 1–3 Pages 94–98.

Sokolov, A. V. and Harris, E. et al. (2001). Femtosecond Light Source for Phase-Controlled Multiphoton Ionization. *Phys. Rev. Lett. 87*, 033402.

Strickland, D. and Mourou, G. (1985). Compression of amplified chirped optical pulses. *Optics Communications 56 3*, 219-221.

Takahashi, E. et al. (2007). Ultra Broadband UV Generation by Stimulated Raman Scattering of Two-color KrF laser in Deuterium Confined in a Hollow Fiber. *Optics Express Vol. 15, No. 5*, 2535-2540.

The Raman Effect. (1998, 12 15). CALCUTTA, West Bengal, India.

Turner, F. C. (2006). *Multifrequency Raman Generation in the Transient Regime.* Waterloo.

Weiner, A. M. (2009). *Ultra-fast Optics.* Wiley.

Yan Y. et al. (1985). Impulsive stimulated scattering: General importance in femtosecond laser pulse interactions with matter, and spectroscopic applications. *Journal of Chemical Physics 83*, 5391-5399.

Yan, H. (2011). *Ultra-short Pulse Generation from Raman Generation.* Waterloo.

Zhavoronkov, N. and Korn, G. (2002). Generation of Single Intense Short Optical Pulses by Ultrafast Molecular Phase Modulation. *Physics Review Letters 88*, 203901.

Zhi, M. and Sokolov, A. . (2012). Toward Single-Cycle Pulse Generation in Raman-Active Crystal. *Selected Topics in Quantum Electronics, IEEE Journal of 18 1*, 460-466.

Appendix: Description of SPIDER Program

The codes related to SPIDER are printed here. All scripts and functions are written in Matlab except the only application in C that reads the spectrometer from GPIB port and stores spectrum. The marked values should be changed once relative configuration is changed.

Phase Retrieving Function

The core program 'spider' is written as a script. Before the starting this script, the following value should be set correctly.

fileName: the path and name of the file. E.g. 'd:\spider\spectrum.txt'

c_lambda: the central wavelength of the target beam

delay: the delay between two pulse replicas

c_f: the center of the frequency filter

n_peak: the index of the pixel of the center frequency

lambda_range: the range of the phase to be calculated in wavelength

```
% set constants and parameters
c = 2.998e8;
i = sqrt(-1);

d_frequency = c * (1/830e-9 - 1/(830e-9+ (363.6364*delay)));


% config wavelength of referencing beam and blue light.
ref_lambda = 830e-9;
c_blue_lambda = 1/(1/c_lambda+1/ref_lambda);



% read spectrum

spectrum_ori = importdata(fileName, ',');
if length(spectrum_ori) ~= 500
    continue
end


%   calibrate the wavelength of spectrometer
c_factor = 6.3025e-012;
lambda_spe_ori = -[1 : 500] * c_factor;
lambda_spe_ori =  lambda_spe_ori + (c_blue_lambda - lambda_spe_ori(n_peak));

% test if the fringes is clear enough
isCoh = isCoherent(lambda_spe_ori, spectrum_ori, c_spe, coh_threshold);


% convert original spectrum to
```

```
% spectrum vs. f with constant interval
% for FFT in next step.
f_ori = c ./ lambda_spe_ori;
[f, spectrum] = getLinear_x_y(f_ori, spectrum_ori);


% apply FFT on spectrum vs. f
Fs_spe = 1/mean(diff(f(1:5)));
NFFT2 = 2^nextpow2(length(spectrum)); % Next power of 2 from length of y
Y = fft(spectrum,NFFT2)/length(spectrum);
f_spe = Fs_spe/2*linspace(0,1,NFFT2/2+1);


% filter out frequencies except those of interests by introduce a 4th power
% Gaussian envelope centered at the frequency of interest
filted_Y= [Y(1:NFFT2/2+1) .* exp(-((f_spe-c_spe)/1.2e-12).^4), zeros(1, NFFT2/2)];
filted_spe = ifft(filted_Y); % get spider spectrum with DC and -AC terms filted out
fined_spe = filted_spe ./ abs(filted_spe) * max(abs(filted_spe));

% select certain (f, spe) data points in filted spider spectrum of interest
[new_f, new_filted_spe, index_range] = selectDomain(f, fined_spe(1:length(f)),
(c./lambda_range + c./ref_lambda));
new_lambda = c ./ new_f;
%
new_omega = c./new_lambda * 2 * pi;
new_omega = new_omega - mean(new_omega);

% get the phase from spider spectrum and substract the linear term
% introduced by delay
dphi = getContinueAngle(angle(new_filted_spe)) - new_omega * delay;
dphi = dphi - mean(dphi);



phi = 1 / d_frequency * mean(diff(new_f(1:5))) * cumtrapz(dphi);
final_f = new_f - c/ref_lambda;
final_lambda = c ./ final_f;
```

Helper Functions for SPIDER

'isCoherent' is a function that returns 1 or 0 to indicate if the fringes is clear enough.

```
function flag = isCoherent(lambda, spe_lambda, c_spe, threshold)

c = 2.998e8;


f_lambda = c ./ lambda;
[f, spe] = getLinear_x_y(f_lambda, spe_lambda);


% apply FFT on spectrum vs. f
Fs_spe = 1/mean(diff(f(1:5)));
NFFT2 = 2^nextpow2(length(spe)); % Next power of 2 from length of y
Y = fft(spe,NFFT2)/length(spe);
f_spe = Fs_spe/2*linspace(0,1,NFFT2/2+1);


[new_f, new_filted_spe, index_range] = selectDomain(f_spe, Y,  [0.25e-11 0.65e-11]);

new_abs_spe = abs(new_filted_spe);

bkg_level = mean([new_abs_spe(1:2), new_abs_spe(end-2:end)]);


coherence = (max(new_abs_spe)/bkg_level);
```

```
flag = (coherence  > threshold);
```

'selectDomain' consumes data points x, y and a range [x'1, x'2] and returns the data points from x, and y with x belongs to range [x'1, x'2].

```
function [new_x, new_y, index_range] = selectDomain(x, y, range)

upper = max(range);
lower = min(range);
n = length(x);
rangeStart = 0;
rangeEnd = 0;
% find the index within the range
for i = 1 : n

    if rangeStart == 0
        flag = ((x(i) > lower) && (x(i) < upper));
        if flag == 1
            rangeStart = i;
        end

    else
        flag = ((x(i) > lower) && (x(i) < upper));

        if flag == 0;
            rangeEnd = i - 1;
            break
        end
    end

end

new_x = x(rangeStart : rangeEnd);
new_y = y(rangeStart : rangeEnd);
index_range = [rangeStart, rangeEnd];
```

Read the oscilloscope

```
/*
 *
 * This application to read from Tektronix TDS Real-Time Oscilloscope
 * using GPIB.
 *
 *
 */
#include <stdio.h>
#include <stdlib.h>
#include <string.h>
#include <conio.h>


int findMaxNum (char *values, int size)
{
        int i,
                strPos = 0, // the index of the current character for mid number string //
                flag = 0,
                maxNum = -100000,  // value of the mid number//
                currentNum = -100000;
        char currentStr[10]= "-1000"; // the string represents the current number //
```

```
        char *pValues; // pointer that points to the current char in values //

        /*      starts from the middle of the string values. find the first number
                enclosed by ',' and ',' */
        for (i = 0; i <  size; i++)
        {

            pValues = values + i;

                flag = (*pValues) == ',';



                if (flag)
                {

                        currentStr[strPos] = '\0';
                        currentNum = atoi(currentStr);

                        strPos = 0;

                        if (currentNum > maxNum)
                        {
                                maxNum = currentNum;

                        }
                }


                else
                {
                        currentStr[strPos] = *pValues;
                        strPos++;
                }
        }
        currentStr[strPos] = '\0';
        if (currentNum > maxNum)
                {
                        maxNum = currentNum;
                }

        return maxNum;
}



#include "ni4882.h"

#define ARRAYSIZE          8192      // Size of read buffer

#define BDINDEX               0      // Board Index
#define PRIMARY_ADDR_OF_SCOPE 1      // Primary address of device
#define NO_SECONDARY_ADDR     0      // Secondary address of device
#define TIMEOUT            T10s      // Timeout value = 10 seconds
#define EOTMODE               1      // Enable the END message
#define EOSMODE               0      // Disable the EOS mode

int  PanelHandle,
     Dev;
char ValueStr[ARRAYSIZE + 1],
     CommandStr[ARRAYSIZE + 1];


int main (int argc, char *argv[])
{
        FILE *f;
        int i = 0;
        int boolean = 0;
        char TestString[7]="curve?";
        char fileName[50];// = "test.txt";
        int totalFile = 100;
```

```
    int maxNum;
    int threshold = -74;

    /* strings for naming the files */
    char prefix[50] = "spider1";
char number[50] = "";
char suffix[10] = ".txt";

    printf("Input file name\n");
    scanf("%s", &prefix);
    printf("Input the number of scans\n");
    scanf("%d", &totalFile);
    printf("Input threshold\n");
    scanf("%d", &threshold);



Dev = ibdev(BDINDEX, PRIMARY_ADDR_OF_SCOPE, NO_SECONDARY_ADDR,
            TIMEOUT, EOTMODE, EOSMODE);

// Clear the internal or device functions of the device.
ibclr (Dev);
    // Set source to channel
    // ibwrt(Dev, )

    while (i < totalFile)
    {
            // write command to retrive data//
            ibwrt (Dev, TestString, strlen(TestString));
            // read data//
            ibrd (Dev, ValueStr, ARRAYSIZE);
            // put an end to the data string //
            ValueStr[ibcntl] = '\0';
            // get the value of the number in the middle of the string //

            maxNum = findMaxNum(&ValueStr, strlen(ValueStr));



            /* drop the data if midNum is below the threshold by starting
            read in new set of data */
            if (maxNum < threshold)
            {
                    continue;
            }

            // generate file name //
            strcpy(fileName, prefix);
     itoa(i+10000, number, 10);
     strcat(fileName, number);
     strcat(fileName, suffix);


            // store data //
            f = fopen(fileName,"w");
            fprintf(f,"%s", ValueStr);
            fclose(f);
            i++;
    }
// write command to get the data//

    ibwrt (Dev, TestString, strlen(TestString));
    // read data//
ibrd (Dev, ValueStr, ARRAYSIZE);


    ValueStr[ibcntl] = '\0';
    fileName[50] = "testosc.txt";
f = fopen(fileName,"w");
    fprintf(f,"%s", ValueStr);
    fclose(f);
```

```
    return 0;
}
```